INTERNATIONAL JOURNAL FOR NUMERICAL METHODS IN ENGINEERING
Int. J. Numer. Meth. Engng 2000; **00**:1–6 *Prepared using* nmeauth.cls *[Version: 2002/09/18 v2.02]*

Hybrid numerical scheme for time evolving wave fields

*G.N.Lilis• A.Halder◇ S.Telukunta† S.Servetto•

Cornell University, Ithaca, NY 14853, USA

KEY WORDS: Finite element method; Inverse problem; Wave field synthesis; Acoustic wave field synthesis; Space-time.

SUMMARY

Many problems in geophysics, acoustics, elasticity theory, cancer treatment, food process control and electrodynamics involve study of wave field synthesis in some form or another. In the present work, modeling of wave propagation phenomena is studied as a static problem, using Finite Element Method and treating time as an additional spatial dimension. In particular wave field synthesis problems are analyzed using discrete methods. It is shown that a fully finite element based scheme is very natural and effective method for the solution of such problems.

Distributed wave field synthesis in the context of two-dimensional problems is outlined and incorporation of any geometric or material non-linearities is shown to be straightforward. This has significant implications for problems in geophysics or biological media, where material inhomogeneities are quite prevalent. Numerical results are presented for several problems referring to media with material inhomogeneities and predefined absorption profiles. The method can be extended to three dimensional problems involving anisotropic media properties in a relatively straightforward manner.

*Correspondence to: • School of Electrical and Computer Engineering, Rhodes Hall † Sibley School of Mechanical and Aerospace Engineering, Upson Hall ◇ Biological and Environmental Engineering, Riley-Robb Hall

Received 1 February 2006
Revised 1 February 2006

Copyright © 2000 John Wiley & Sons, Ltd.

1. Introduction

The area of wave field synthesis is a broad one that has applications in various diverse fields like geophysics [26], indoor acoustics [6], elasticity theory [23, 25], cancer treatment, food process control [27] and elastodynamics [24].

One form of cancer treatment is interstitial thermal therapy which is also called hyperthermia. This refers to the use of various heat generating sources to be injected into the body and selectively raise the temperature of a local tissue region. The method offers the promise of becoming an alternative to surgery, radiation therapy and chemotherapy [19, 20]. Its applications refer to the treatment of certain localized malignancies like brain tumors [15] and prostate cancer [13, 14]. The treatment protocol involves placing needle-based energy sources directly in the tumor and increasing the tissue temperature to cause cell death. The energy sources available for interstitial thermal therapy include radio frequency electrodes, microwave antennas, ultrasound transducers and laser fiber optics [16]. Of these, the largest technological and clinical experience has been with radio frequencies and microwave applicators [17],[12]. Using these techniques one can cure tumors up to approximately $3cm$ in diameter. Microwave antennas launch electromagnetic waves in the frequency range of 300 MHz to 2450 MHz in the surrounding tissue. The waves propagate and interact with each other causing small currents to flow locally as they propagate. These local currents produce heating of the tissue due to the resistance of the tissue and increase the local temperature which depends on the intensity of the wave.

The volume of tissue that can be heated with a single thin antenna is usually small, and therefore, arrays of several antennas with precisely controlled field generation are required to destroy an entire tumor [18]. However, placement of these antennas with accurate field evolution is essential to produce the desired effects and wave field synthesis provides a way of analyzing this problem. Currently, forward analysis with the two-dimensional finite element/finite difference method is widely used to solve the wave propagation problem. This forward analysis method derives the temperature distribution for a given electrode configuration by solving the wave equation and then the bio-heat transfer equation. This analysis requires modification of the electrode configuration by trial and error to reach an optimum configuration for better temperature distribution [21]. This type of analysis does not give an optimal heating condition directly. Wave field synthesis provides a convenient way to overcome the above mentioned difficulty. The present paper is applicable to the field synthesis and hence addresses a part of this problem.

Acoustic wave field analysis or simply wave field analysis (WFA) refers to the recording of sound fields in enclosures with arrays of microphones and to the processing of the recorded data. Acoustic wave field synthesis or simply wave field synthesis (WFS) refers to the generation of sound fields with desired or prescribed temporal and spatial properties. The idea of wave field synthesis has been in existence for many years, and is often credited to have been first introduced by Berhkout in 1988 [1],[5]. Its theoretical foundation is related with the Huygens' principle [22]. A good introductory review of this literature can be found in [3],[4].

In traditional applications of sound enhancement or reproduction, individual or groups of loudspeakers are used to generate a replica of the desired sound pattern [2]. Use of high-quality systems in appropriate manner will help in generation of required temporal properties of sound, however the spatial properties are determined by the interference patterns and often the spatial signal is correct only within a very limited listener area. As an example, consider

the use of two loud speakers to enhance the signal of a primary point source behind them. Most listeners perceive the signal of the loudspeakers earlier than the primary signal which leads to mislocalization, since the first arriving sound wave determines the direction from which the sound is heard. Another drawback of the traditional approach of sound reproduction, is that the sound field is measured first, at a few chosen "representative" positions, assuming that the acoustic parameters (sound speed, attenuation) are valid for some (usually) large region around these points. This, however, is not a reliable approach as it does not include the spatial and temporal inhomogeneities of the acoustic medium.

In the current state of the art, these problems are overcome with the use of array technology involving the use of arrays of microphones and micro-speakers. These are placed at suitable positions either on the boundary or within an enclosed volume. Then techniques based on the wave field synthesis (WFS) and the wave field analysis (WFA) involving a significant amount of experimentation and hence considerable cost, are used. In the present work, a numerical technique using continuous interpolations both in space and time is developed, in order to carry out the procedure of wave field synthesis. Space-time techniques for solving elastodynamic and wave propagation problems have been studied in the past by Hulbert and Hughes [7],[8],[11]. Galerking methods have been applied to hyperbolic problems with the use of basis functions that are continuous in space but discontinuous in time by Johnson [9].

A short description of the wave field synthesis problem is as follows. Given a complete description in space and time of a scalar wave field $\Phi(x, y, z, t)$ inside a spatial region S, specify a source function $F(x, y, z, t)$, distributed at specific points in this region, which creates a field as similar as possible to the previous field. In the present work we investigate the effectiveness of finite element method applied to wave field synthesis problems that are two dimensional.

The paper is organized as follows. First, preliminary definitions are postulated. Then a 2-D wave field model both in continuous and in matrix form is described. Based on this model a formal definition of a distributed wave field synthesis problem is presented together with a numerical solution technique. The paper concludes with several examples of wave field synthesis applied in various simple domains. The effect of domain partition and the induced error is studied in detail as well.

2. Preliminaries and modeling

2.1. Preliminary definitions

Consider wave propagation inside a 2 dimensional, inhomogeneous medium (spatial region S with boundary ∂S) with geometrical characteristics defined by a subset $S \subset \mathbf{R}^2$ and properties (modulus of elasticity k, density ρ and absorption coefficient a) which are functions of both space and time [3],[5]. Additionally consider $[0, T]$ to be the time interval of interest.
Under the above assumptions we can make the following definitions:

Definition 1: *Continuous space-time domain as the following cartesian product:* $\Omega = S \times [0, T]$.

Definition 2: *Cubic space-time elemental domain or sub-domain* $\Delta\Omega^{(n)}$ *having as origin the point* (x_n, y_n, t_n) *and sides* ΔX, ΔY *and* ΔT *as the following set:*

$$\Delta\Omega^{(n)} = [x_n, x_n + \Delta X] \times [y_n, y_n + \Delta Y] \times [t_n, t_n + \Delta T] \tag{1}$$

Definition 3: *Square space-time surfaces are boundary surfaces of the elemental domain* $\Delta\Omega^{(n)}$ *defined as:*

$$\begin{aligned}
\Delta S^{(n)}_{-x} &= \{x_n\} \times [y_n, y_n + \Delta Y] \times [t_n, t_n + \Delta T] \\
\Delta S^{(n)}_{+x} &= \{x_n + \Delta X\} \times [y_n, y_n + \Delta Y] \times [t_n, t_n + \Delta T] \\
\Delta S^{(n)}_{-y} &= [x_n, x_n + \Delta X] \times \{y_n\} \times [t_n, t_n + \Delta T] \\
\Delta S^{(n)}_{+y} &= [x_n, x_n + \Delta X] \times \{y_n + \Delta Y\} \times [t_n, t_n + \Delta T] \\
\Delta S^{(n)}_{-t} &= [x_n, x_n + \Delta X] \times [y_n, y_n + \Delta Y] \times \{t_n\} \\
\Delta S^{(n)}_{+t} &= [x_n, x_n + \Delta X] \times [y_n, y_n + \Delta Y] \times \{t_n + \Delta T\}
\end{aligned} \tag{2}$$

Definition 4: *Partition of the space time domain* Ω *into* N *space-time elemental domains* $\Delta\Omega^{(n)}_{n=1,...,N}$ *is defined as the union of* N *disjoint space-time elemental domains* $\bigcup_{n=1}^{N} \Delta\Omega^{(n)}$ *satisfying the following properties:*

1. $\Omega \subset \bigcup_{n=1}^{N} \Delta\Omega^{(n)}$
2. No elemental domain $\Delta\Omega^{(m)}$ with origin the point (x_m, y_m, t_m) can be contained in the remaining set $\bigcup_{n=1}^{N} \Delta\Omega^{(n)} - \Omega$. In other words $\nexists (x_m, y_m, t_m) \in \bigcup_{n=1}^{N} \Delta\Omega^{(n)} - \Omega : \Delta\Omega^{(m)} \subseteq (\bigcup_{n=1}^{N} \Delta\Omega^{(n)} - \Omega)$
3. *If the intersection between any two elemental domains from the set* $\{\Delta\Omega^{(n)}\}_{n=1,...,N}$ *is not empty then this intersection is one of the space-time surfaces defined in definiton 3 which belongs to both of the elemental domains.*

Definition 5: *Orthogonal grid of points* Ω_G *given a partition* $\bigcup_{n=1}^{N} \Delta\Omega^{(n)}$ *defined in 4 is a set of* G *global space-time points* $\Omega_G = \{(x_g, y_g, t_g)_{g=1,...,G} \in \Omega\}$ *that are defined by the apexes of the elemental domains* $\{\Delta\Omega^{(n)}\}_{n=1,...,N}$*, namely:* $\{x_n, x_n + \Delta X, y_n, y_n + \Delta Y, t_n, t_n + \Delta T\}_{n=1,...,N}$

Definition 6: *Boundary sets of surfaces* $N_{\pm x}, N_{\pm y}, N_{\pm t}$ *of a partition* $\bigcup_{n=1}^{N} \Delta\Omega^{(n)}$ *of a domain* Ω *are surfaces of the elemental domains* $\Delta\Omega^{(n)}$ *defined in 3 which satisfy:*

$$\begin{aligned}
N_{\pm x} &= \{n \in \{1, ..., N\} : \quad \forall m \in 1, ..., N \quad \Delta S^{(n)}_{\pm x} \neq \Delta S^{(m)}_{\pm x}\} \\
N_{\pm y} &= \{n \in \{1, ..., N\} : \quad \forall m \in 1, ..., N \quad \Delta S^{(n)}_{\pm y} \neq \Delta S^{(m)}_{\pm y}\} \\
N_{\pm t} &= \{n \in \{1, ..., N\} : \quad \forall m \in 1, ..., N \quad \Delta S^{(n)}_{\pm t} \neq \Delta S^{(m)}_{\pm t}\}
\end{aligned} \tag{3}$$

2.2. Continuous form of the wave PDE at the element level

Based on the above definitions, and considering an acceptable degree of approximation, at every space-time point $(x, y, t) \in \Delta\Omega^{(n)}$ the properties of the medium can be assumed to be constant. More precisely, in acoustics and in mechanics generally, the modulus of elasticity $k(x, y, t)$, the density $\rho(x, y, t)$ and the absorption coefficient $a(x, y, t)$, may satisfy:

$$\forall (x, y, t) \in \Delta\Omega^{(n)} : \quad k(x, y, t) \approx k_n, \quad \rho(x, y, t) \approx \rho_n, \quad \alpha(x, y, t) \approx \alpha_n \tag{4}$$

Therefore inside such a domain the 2 dimensional wave partial differential equation that relates the wave field function $\Phi(x, y, t)$ with the source function $F(x, y, t)$, can be assumed to be satisfied, namely:

$$k_n[\Phi_{xx} + \Phi_{yy}] - \rho_n \Phi_{tt} - a_n \Phi_t = -F \qquad \text{with} \qquad \Phi_{xx} = \frac{\partial^2 \Phi}{\partial^2 x} \quad \Phi_{yy} = \frac{\partial^2 \Phi}{\partial^2 y} \quad \Phi_{tt} = \frac{\partial^2 \Phi}{\partial^2 t} \tag{5}$$

The form in (5) is the **continuous form** of the wave equation which is satisfied at the points of the elemental domain $\Delta\Omega^{(n)}$. However in the next sections we make use of a **matrix form** of the same equation for the points of the orthogonal grid Ω_G. The derivation of this matrix form is presented in Appendix A.

2.3. Matrix form of the wave PDE

Given an orthogonal grid of G space-time points defined in definition 5 and following the procedure described in Appendix A, a linear system that governs the relationship between the values of a wave field Φ at these space-time points (contained in the vector $\{\Phi^{(G)}\}$) and the values of a source function generating the previous field at these points (contained in the vector $\{F^{(G)}\}$) can be obtained. This system is call the matrix form of the Wave PDE and can be expressed by:

$$[K_{G\times G}]\{\Phi^{(G)}\} + \{F^{(G)}\} = 0 \tag{6}$$

Based on the previous linear system, a formal definition of a distributed wave field synthesis problem is postulated and a numerical solution technique is described.

3. Distributed Wave Field Synthesis - dWFS

Wave field synthesis problems or WFS are problems that refer to the synthesis of certain known field functions $\Phi(x, y, t)$ in a specific space-time domain Ω by means of a source function $F(x, y, t)$ that has to be specified. For more details on these problems refer to [1, 2]. Such problems appear also as inverse wave field problems [29], as opposed to direct wave field problems in which the field is the unknown parameter and not the source function. A distributed wave field synthesis problem, or dWFS [30], is a problem in which both the field and the source functions are described only in a finite set of points Ω_G, as opposed to the classical WFS problems where both functions are described in the whole domain Ω. Usually in dWFS problems the values of both the source and the field function at the points of Ω that are not grid points are derived using linear interpolation based on the values of these functions

at the grid points. There are two versions of dWFS problems. The ideal and the constrained version, which will be analyzed next.

3.1. Ideal distributed wave field synthesis problem

Generally, a wave field synthesis problem or an inverse wave problem can be formulated as follows. Given a medium, geometrically defined by a set $S \subset \mathbf{R}^2$ with boundaries ∂S which has properties (density ρ, modulus of elasticity k and absorption coefficient α), a time interval $[0, T]$ and assuming a time evolving scalar field $\Phi(x, y, t)$ satisfying the equation:

$$k[\Phi_{xx} + \Phi_{yy}] - \rho\Phi_{tt} - a\Phi_t = -F, \qquad \forall(x, y) \in S \quad \forall t \in T \tag{7}$$

specify the source function $F(x, y, t)$ that produces the field distribution $\Phi(x, y, t)$.

An important observation that can be derived from the above formulation is that the resulting source function will not necessarily have to reside in one specific region or act at specific time intervals, hence can be distributed in both space and time. These ideas lead us to define a new family of WFS problems called distributed WFS problems or dWFS.

Compared with the classical WFS problems, dWFS refer to partitioned domains Ω_G (according to definition 5) defined by space time points, $\omega_g = (x_g, y_g, t_g)$. These triplets are apexes of elemental cubes. Therefore as an introductory example, lets consider a simple case of a medium where 18 space time points are defined (9 space points for each of the two time frames) as displayed in figure 3.1.

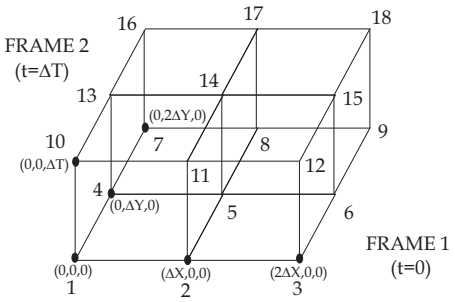

Figure 1. Partitioned space time domain of 2 frames of 9 points each

Given the above partition and based on the mathematical derivations in Appendix A a linear relation between the values of the field Φ and the values of the source F at the above space time points can be obtained:

$$[K^{(G)}_{18\times18}]\{\Phi^{(G)}_{18\times1}\} + \{F^{(G)}_{18\times1}\} = 0, \tag{8}$$

where $\{\Phi^{(G)}_{18\times1}\}$ is a 18x1 vector containing in the first 9 entries the field values at the space-time points of the first frame and in the next 10-18 entries the field values at the space-time points of the second frame. In the same manner the vector $\{F^{(G)}_{18\times1}\}$ contains the respective

source values at the same space-time points.

In a more general context and considering a finer partition for the same domain, the number of space time points is much larger. Assuming F frames and P space points at each frame we will have a set $\{1, ..., G\}$ of $G = FP$ space-time points. Therefore, generally a $G \times G$ system expressing the coupling between the field and source values at these G space-time points can be written as:

$$[K^{(G)}_{G\times G}]\{\Phi^{(G)}_{G\times 1}\} + \{F^{(G)}_{G\times 1}\} = 0 \tag{9}$$

Based on this formulation and the knowledge of field values at these specific points, it makes sense to evaluate the source function at the same points, by solving directly the system for the vector $\{F^{(G)}_{G\times 1}\}$.

$$\{F^{(G)}_{G\times 1}\} = -[K^{(G)}_{G\times G}]\{\Phi^{(G)}_{G\times 1}\} \tag{10}$$

In this case the $\{F^{(G)}_{G\times 1}\}$ vector contains the values of the required source signals that must be applied at the G space-time points. In other words this direct solution describes the amplitudes at specific locations and time instances of the source function F that produces the field values contained in $\{\Phi^{(G)}_{G\times 1}\}$.

However very often, a source residing at specific locations and acting at time intervals specified by the direct solution (10), is not physically realizable. For example in ultrasound cancer treatment, placing sources inside the patient's body is impossible.

Therefore we have to impose certain constraints referring to where and when the source should act. Consequently, a different problem referring to the spatial and temporal constraints of the source function is formulated. This problem is analyzed in the next section.

3.2. Distributed wave field synthesis problem with source constraints

A distributed wave field synthesis problem with source constraints is essentially a dWFS problem with additional spatial and temporal constraints in the source function $F(x, y, t)$. We can view these constraints as regions of the space-time orthogonal grid Ω_G where the function is allowed to take non zero values. Equivalently, these constraints can be described by a null set or a subset of Ω_G where the function F is forced to be zero. More precisely:

Definition 7*: Null set Ω_F of a constrained source function $F(x, y, t)$ is a subset of the orthogonal grid of points Ω_G, defined in definition 5, satisfying:*

$$\Omega_F = \{(x_g, y_g, t_g) \in \Omega_G : \quad F(x_g, y_g, t_g) = 0\} \tag{11}$$

Having defined the null set of a source function we can postulate the definition of a dWFS problem with source constrains as follows:

Given:

[1] An isotropic spatial medium geometrically defined by a set $S \subset \mathbf{R}^2$ with boundaries ∂S which has certain properties (density $\rho(x, y, t)$, modulus of elasticity $k(x, y, t)$ and absorption coefficient $a(x, y, t)$) and a time interval $[0, T]$ which together with S define a domain $\Omega = S \times [0, T]$.

[2] An orthogonal grid of points Ω_G that defines a partition of the domain Ω according to definition 5.

[3] A partition of Ω_G into two disjoint subsets Ω_1 and Ω_2 ($\Omega_G = \Omega_1 \cup \Omega_2$ and $\Omega_1 \cap \Omega_2 = \emptyset$).

[4] The information of a time evolving scalar field $\Phi(x, y, t)$ at the space-time points of Ω_G as values $\{\Phi(x_g, y_g, t_g) : (x_g, y_g, t_g) \in \Omega_G\}$ which are contained in a vector $\{\Phi^{(G)}\}$.

Specify:

The values of a constrained source function F_c with null set $\Omega_{F_c} = \Omega_2$, as a vector $\{F_c^{(G)}\}$ such that the following quantity is minimized

$$||\{\Phi^{(G)}\} - \{\Phi_c^{(G)}\}||_2 = \min \tag{12}$$

subject to the matrix form of the wave PDE, which relates the values of this source $\{F_c^{(G)}\}$ to the values of the field it creates $\{\Phi_c^{(G)}\}$:

$$[K_{G\times G}^{(G)}]\{\Phi_c^{(G)}\} + \{F_c^{(G)}\} = 0 \tag{13}$$

The notation $||.||_2$ is used to represent the second norm of a vector, or the square root of the sum of the squares of its entries.

It is easy to comprehend the previous formulation through an example. Consider a two dimensional elliptical region S consisting of two subregions S_1 and S_2. The continuous and the partitioned versions of these regions are displayed in figure 2. Also assume that $S = S_1 \cup S_2$ and $S_1 \cap S_2 = \emptyset$.

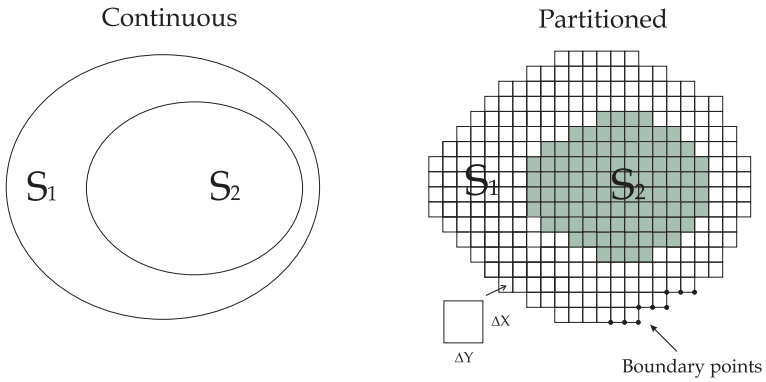

Figure 2. Continuous and partitioned elliptical 2D region

Now consider the same divided 2D space region S as it "evolves" during a specific time interval $[0, T]$, $T > 0$. In other words consider the space-time points (x, y, t) where $(x, y) \in S$

and $t \in [0, T]$. Then the created space-time domain $\Omega = S \times [0, T]$ will obtain a cylindrical like shape as figure 3 depicts. Following also the partition of the region S into S_1 and S_2 and assuming that the boundary between the regions S_1 and S_2 does not change with time, the domain Ω can be partitioned into two sub-domains $\Omega_1 = S_1 \times [0, T]$ and $\Omega_2 = S_2 \times [0, T]$ as in figure 3.

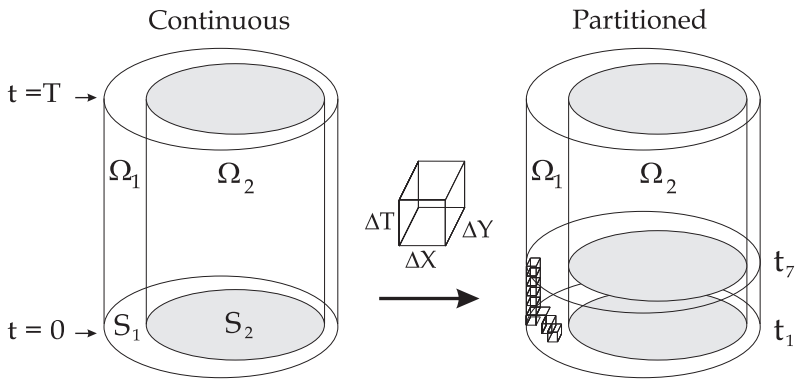

Figure 3. Continuous and partitioned domain Ω

An example of such a configuration might be a cross section of a human body having a tumor in the region S_2 and the only feasible locations to place microwave sources are points in region S_1. Therefore by letting the sources reside only in S_1 and act at every time instance in $[0, T]$, is equivalent with forcing the null set of the constrained source function $\{F_c\}$ to be the sub-domain $\Omega_2 = S_2 \times [0, T]$.

In order to pass from a continuous domain to a partitioned domain, space time elemental domains described in definition 2 must be used. A time step or a "side" in the time axis of these elemental domains ΔT must be chosen. If the time step is the same for all the elemental domains then it must be equal to $\Delta T = \frac{T}{F-1}$ where F is the total number of frames t_f, $f = 1, ..., F$, including the first one. The partition in space remains the same as presented in figure 2. By the apexes of the resulting elemental domains a grid of G space time points is defined following definition 5. Then both the source and the field functions are described as vectors, containing their values at the space-time points defined by the previous grid, namely:

$$\{\Phi^{(G)}\} = \{\Phi(x_g, y_g, t_g)\}_{g=1,...,G} \qquad \{F^{(G)}\} = \{F(x_g, y_g, t_g)\}_{g=1,...,G} \tag{14}$$

For the configuration of this example a constrained dWFS problem might described as follows. Given a destructive for the tumor field $\{\Phi^{(G)}\}$ (having big values in Ω_2) specify a constrained source $\{F_c^{(G)}\}$ with null set the grid of points that belong to Ω_2, such that the error between the field it creates $\{\Phi_c^{(G)}\}$ and the original field $\{\Phi^{(G)}\}$ ($||\{\Phi_c^{(G)}\} - \{\Phi^{(G)}\}||_2$) is minimized.

4. Solution to the dWFS problem

4.1. Vector and matrix rearrangement

In order to solve a dWFS problem a partition of the space-time domain Ω must be done, which will create a grid of finite points according to definition 5. Then a division of the resulting finite set of the grid points into two subsets Ω_1 and Ω_2 must be applied. An example of such partition and division of an orthogonal grid is displayed in figure 3.
According to this division and based on the results of Appendix A, the entries of the vectors $\{\Phi^{(G)}\}$ and $\{F^{(G)}\}$ and the matrix $[K_{G\times G}]$ of equation 6 can be separated as follows.
If the base points of region S (points of the first frame in figure 2) are P then the first P entries of the vectors $\{\Phi\}$ and $\{F\}$ will refer to the first P values of the field and the source function at the first frame. The next P to the second frame etc. Now lets assume that B of the P base points refer to the boundary of the base and I of the P base points refer to the inner points of the base, as figure 2 displays. Then clearly $P = B + I$. If now region S_1 has I_1 inner points and region S_2, I_2 then the sum of the inner points of the two regions must be equal to the total inner points of the base, namely $I_1 + I_2 = I$. Therefore for the base points of the first frame it must be: $I_1 + I_2 + B = P$. By applying appropriate labeling in the points of the first frame, the first I_1 inner points of the first frame which also are inner points of the first region S_1 will refer to the first I_1 entries of the vectors $\{\Phi\}$ and $\{F\}$. Following the same idea the next I_2 inner points of the first frame which are also the inner points of the second region will refer to the next I_2 entries of the vectors $\{\Phi\}$ and $\{F\}$. Finally the remaining B boundary points of the first frame will refer to the next B entries of the vectors $\{\Phi\}$ and $\{F\}$. Following this method the remaining entries of the vectors $\{\Phi\}$ and $\{F\}$ will be associated with the respective points of the second, third,...,F frame. Figure 4 refers to such arrangement.

Then if the entries in the two previous vectors are rearranged in a way that the first FI_1 entries refer to region S_1 for all the frames and the next FI_2 refer to S_2 for all the frames and the last FB refer to the boundary points for all the frames, then the source vector $\{F\} = \{f_1, ..., f_G\}$, $G = FP$ will obtain a form that is displayed in figure 5 (The rearrangement for the field vector $\{\Phi\}$ follows the same pattern):

The new form of system (6) after the rearrangement of the vectors $\{\Phi^{(G)}\}$ and $\{F^{(G)}\}$ will include also rearrangement of rows and columns of the $[K_{G\times G}]$ matrix:

$$\begin{bmatrix} K_{11} & K_{12} & K_{1B} \\ K_{21} & K_{22} & K_{2B} \\ K_{B1} & K_{B2} & K_{BB} \end{bmatrix} \begin{Bmatrix} \Phi_1 \\ \Phi_2 \\ \Phi_B \end{Bmatrix} + \begin{Bmatrix} F_1 \\ F_2 \\ F_B \end{Bmatrix} = 0 \tag{15}$$

The sub matrices K_{11} and K_{22} refer to the inner points of the sub-domains Ω_1 and Ω_2 and they have dimensions $I_1F \times I_1F$ and $I_2F \times I_2F$ respectively, while the sub-matrices K_{12} and K_{21} refer to the boundary between the previous two sub-domains and have dimensions $I_1F \times I_2F$ and $I_2F \times I_1F$ respectively. The sub-matrix K_{BB} refers to the boundary points and has dimension $BF \times BF$. Finally, the sub-matrices K_{1B}, K_{2B} , K_{B1} and K_{B2} have dimensions $I_1F \times BF$, $I_2F \times BF$, $BF \times I_1F$ and $BF \times I_2F$ respectively. The association between this matrix, vector division and the domain division is displayed in figure 6.

Part of the previous system that refers to the inner points of the domain Ω can be written as:

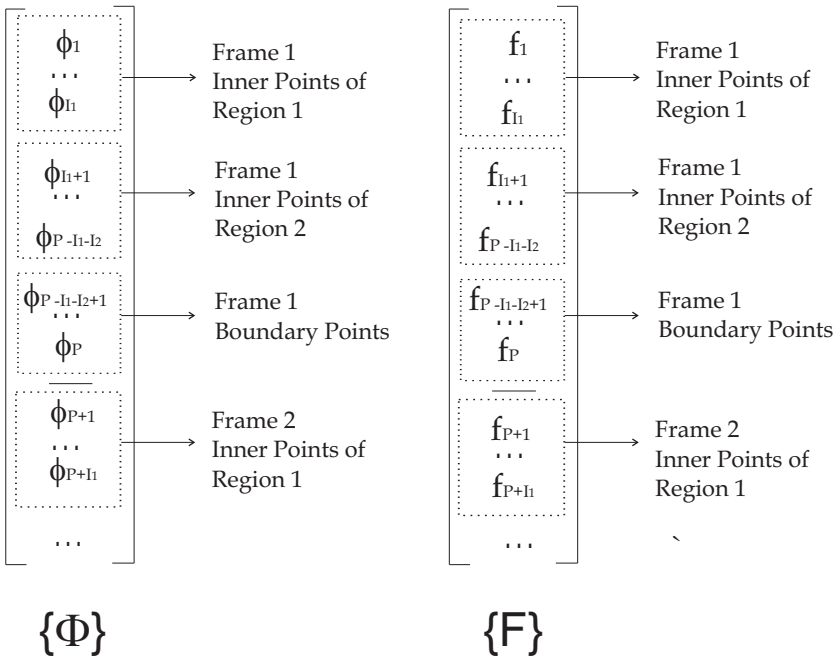

Figure 4. Initial arrangement of source and field vectors

$$\begin{bmatrix} K_{11} & K_{12} \\ K_{21} & K_{22} \end{bmatrix} \begin{Bmatrix} \Phi_1 \\ \Phi_2 \end{Bmatrix} + \begin{Bmatrix} F_1 + [K_{1B}]\{\Phi_B\} \\ F_2 + [K_{2B}]\{\Phi_B\} \end{Bmatrix} = 0 \tag{16}$$

The part that is left refers to the boundary points and can be written as:

$$[K_{B1}]\{\Phi_1\} + [K_{B2}]\{\Phi_2\} + [K_{BB}]\{\Phi_B\} + \{F_B\} = 0 \tag{17}$$

System 16 refers to the inner points of the sub-domains Ω_1 and Ω_2 since we exclude all the boundary points.

The main reasons why the boundary points are excluded are the following:

- The matrices $[K_{11}]$ and $[K_{22}]$ are non-singular and therefore good for any matrix operations.
- Many problems refer to synthesis of wave fields in a region that doesn't have any boundary points and therefore the values of the field at these points are not very important.

Equations like (16) can be written also for the constrained source F_c and the field it creates Φ_c given that the constrained source at the inner points of the domain Ω_2 is zero (equivalently $F_{c2} = 0$). Therefore:

$$\begin{bmatrix} K_{11} & K_{12} \\ K_{21} & K_{22} \end{bmatrix} \begin{Bmatrix} \Phi_{c1} \\ \Phi_{c2} \end{Bmatrix} + \begin{Bmatrix} F_{c1} + [K_{1B}]\{\Phi_{cB}\} \\ 0 + [K_{2B}]\{\Phi_{cB}\} \end{Bmatrix} = 0 \tag{18}$$

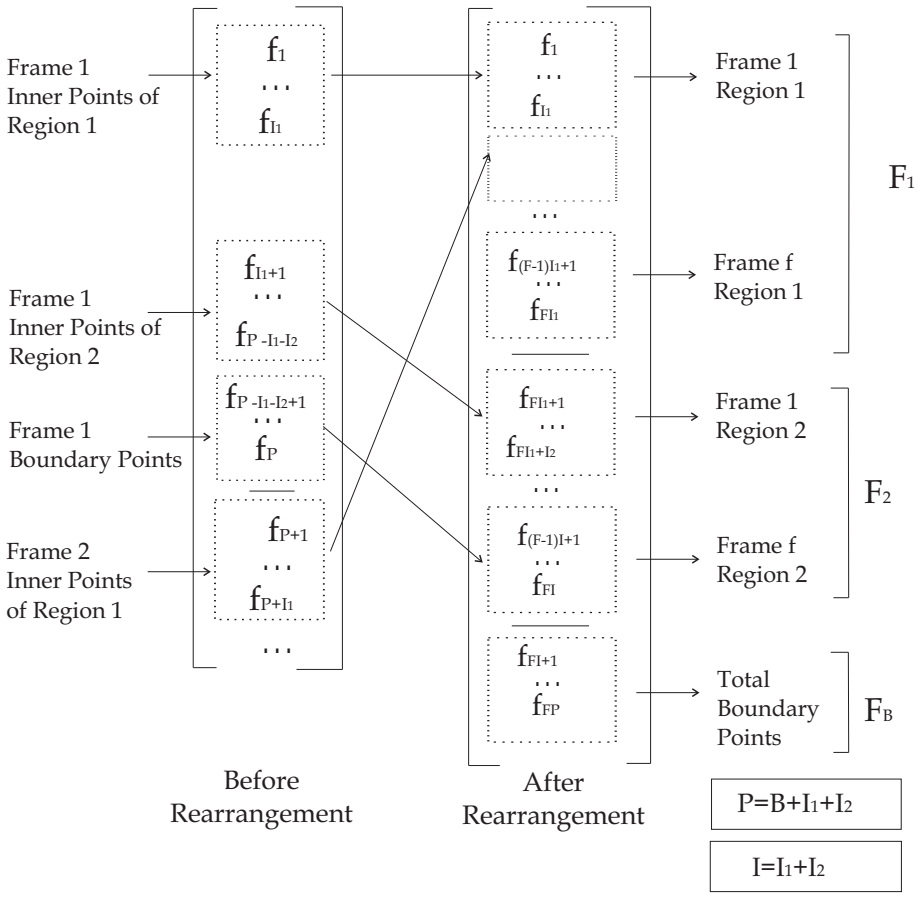

Figure 5. Rearrangement of source vector

with boundary equation:

$$[K_{B1}]\{\Phi_{c1}\} + [K_{B2}]\{\Phi_{c2}\} + [K_{BB}]\{\Phi_{cB}\} + \{F_{cB}\} = 0 \tag{19}$$

Taking the difference of the systems (16) and (18) yields:

$$\begin{bmatrix} K_{11} & K_{12} \\ K_{21} & K_{22} \end{bmatrix} \begin{Bmatrix} \Phi_1 - \Phi_{c1} \\ \Phi_2 - \Phi_{c2} \end{Bmatrix} + \begin{Bmatrix} F_1 - F_{c1} + [K_{1B}]\{\Phi_B - \Phi_{cB}\} \\ F_2 + [K_{2B}]\{\Phi_B - \Phi_{cB}\} \end{Bmatrix} = 0$$

or

$$[K_{11}]\{\Phi_1 - \Phi_{c1}\} + [K_{12}]\{\Phi_2 - \Phi_{c2}\} = \{F_{c1}\} - \{F_1\} - [K_{1B}]\{\Phi_B - \Phi_{cB}\}$$
$$[K_{21}]\{\Phi_1 - \Phi_{c1}\} + [K_{22}]\{\Phi_2 - \Phi_{c2}\} = -\{F_2\} - [K_{2B}]\{\Phi_B - \Phi_{cB}\}$$

For the boundary points:

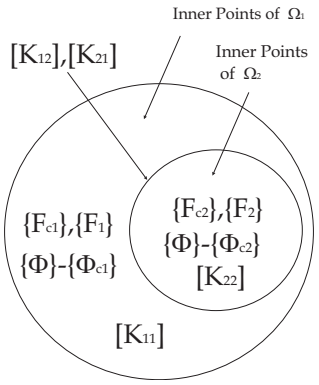

Figure 6. Matrix, vector and domain division

$$[K_{B1}]\{\Phi_1 - \Phi_{c1}\} + [K_{B2}]\{\Phi_2 - \Phi_{c2}\} + [K_{BB}]\{\Phi_B - \Phi_{cB}\} = \{F_{cB}\} - \{F_B\} \tag{20}$$

4.2. Least squares error method

Now in order to solve the previous system for the constrained source vector $\{F_{c1}\}$ the following optimization technique can be applied:

Step 1. We define the error vectors $\{e_1\}$, $\{e_2\}$ and $\{e_B\}$, between the field vector $\{\Phi\}$ and the constrained field vector $\{\Phi_c\}$ at the inner points of the sub-domains Ω_1 and Ω_2 and at the boundary points, respectively as:

$$\{e_1\} = \{\Phi_1\} - \{\Phi_{c1}\} \qquad \{e_2\} = \{\Phi_2\} - \{\Phi_{c2}\} \qquad \{e_B\} = \{\Phi_B\} - \{\Phi_{cB}\} \tag{21}$$

Based on this, the total square error in the inner space-time points of the whole domain Ω can be defined as:

$$\begin{aligned} E &= \{e_1\}^T\{e_1\} + \{e_2\}^T\{e_2\} \\ E &= [\{\Phi_1\} - \{\Phi_{c1}\}]^T[\{\Phi_1\} - \{\Phi_{c1}\}] + [\{\Phi_2\} - \{\Phi_{c2}\}]^T[\{\Phi_2\} - \{\Phi_{c2}\}] \end{aligned} \tag{22}$$

Step 2. After the definitions of the error vectors the system (20) becomes:

$$\begin{aligned} [K_{11}]\{e_1\} + [K_{12}]\{e_2\} &= \{F_{c1}\} - \{F_1\} - [K_{1B}]\{e_B\} \\ [K_{21}]\{e_1\} + [K_{22}]\{e_2\} &= -\{F_2\} - [K_{2B}]\{e_B\} \end{aligned} \tag{23}$$

Now since we have the freedom of choosing the values of the constrain source at the boundaries ($\{F_{cB}\}$) we can force the boundary error vector to take zero values ($\{e_B\} = 0$). Then utilizing (20) we can calculate the required constrained source values at the boundary:

$$\{F_{cB}\} = [K_{B1}]\{e_1\} + [K_{B2}]\{e_2\} + \{F_B\} \tag{24}$$

After setting $\{e_B\} = 0$ and solving system (23) for the vectors $\{e_1\}$ and $\{e_2\}$ will yield:

$$\begin{aligned}
&\{e_1\} = [A]\{F_{c1}\} + \{b\} \\
&\{e_2\} = [C]\{F_{c1}\} + \{d\} \\
&[A] = [[K_{11}] - [K_{12}][K_{22}]^{-1}[K_{21}]]^{-1} \qquad \{b\} = [A][[K_{12}][K_{22}]^{-1}\{F_2\} - \{F_1\}] \\
&[C] = -[K_{22}]^{-1}[K_{21}][A] \qquad\qquad\qquad\quad \{d\} = -[K_{22}]^{-1}[\{F_2\} + [K_{21}]\{b\}]
\end{aligned} \tag{25}$$

Step 3 Now utilizing (25)) and (22) we are able to express E as a function of the vector $\{F_{c1}\}$:

$$\begin{aligned}
&E = \{F_{c1}\}^T[H]\{F_{c1}\} + \{F_{c1}\}^T\{L\} + \{L\}^T\{F_{c1}\} + m \\
&[H] = [A]^T[A] + [C]^T[C] \\
&\{L\} = [A]^T\{b\} + [C]^T\{d\}
\end{aligned} \tag{26}$$

Since the expression for E is convex with respect to $\{F_{c1}\}$ and since we want to minimize it, a straightforward approach is to look for $\{F_{c1}\}^*$ such that:

$$\frac{\partial E}{\partial \{F_{c1}\}}\Big|_{\{F_{c1}\}=\{F_{c1}\}^*} = 0 \tag{27}$$

After forcing the above derivative to be zero we calculate:

$$\{F_{c1}\}^* = -[H]^{-1}\{L\} = -[[A]^T[A] + [C]^T[C]]^{-1}[[A]^T\{b\} + [C]^T\{d\}] \tag{28}$$

4.3. Variable weights

In the previous approach a minimization of the sum of the square error E at each inner space-time point was attempted. However, in some applications we can allow to have bigger errors at some space-time nodes while at others we want to be more accurate or have less error. Therefore instead of trying to minimize a simple error sum given by (22) we can minimize a weighted error expression given by:

$$E' = \{e_1'\}^T\{e_1'\} + \{e_2'\}^T\{e_2'\} \qquad \{e_1'\} = \{w_1\}^T\{e_1\} \qquad \{e_2'\} = \{w_2\}^T\{e_2\} \tag{29}$$

It is very easy to show that the analysis remains the same by replacing the matrices $[A], [C]$ and the vectors $\{b\}, \{d\}$ with:

$$[A'] = \{w_1\}[A] \qquad [C'] = \{w_2\}[C] \qquad \{b'\} = \{w_1\}^T\{b\} \qquad \{d'\} = \{w_2\}^T\{d\} \tag{30}$$

where $\{w_1\}$ are $\{w_2\}$ weighting vectors satisfying:

$$\sum_{i=1}^{|w_1|} w_1(i) + \sum_{i=1}^{|w_2|} w_2(i) = |w_1| + |w_2| \qquad w_k(i) \geq 0 \quad k = 1, 2 \qquad i = 1, ..., |w_k| \tag{31}$$

Therefore, the solution for the constrained source vector will be given by:

$$\{F_{c1}\}^* = -[H']^{-1}\{L'\} = -[[A']^T[A'] + [C']^T[C']]^{-1}[[A']^T\{b'\} + [C']^T\{d'\}] \tag{32}$$

4.4. Error quantification

From the above analysis we can clearly express the relationship between source function values and the field values at specific space-time nodal points. Furthermore, a linear interpolation for both source function and field function must be used in order to find out the values of these functions at any other space-time points apart from the grid space-time points. These interpolations, introduce error which cannot be avoided since we have not complete knowledge of the field and the source function at any given space-time point. For one time instant and for a square elemental domain with "space" sides $\Delta X = \Delta Y = \alpha$, the interpolation is illustrated by figure 7.

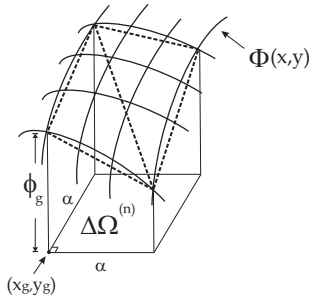

Figure 7. Linear interpolation of the field values at one time instant at a specific elemental domain

As we see the error is introduced by the difference between the curved surface created by the values of the scalar field and the plane surfaces passing through the points (x_g, y_g) defined by the heights ϕ_g. These heights are equal to the values of the field at the points (x_g, y_g). Assuming that the scalar field function Φ is continuous with respect to x and y and by choosing the sides of the square elemental domains small enough we can argue that the previously described error can be diminished. A complete analysis of this error as a function of the spectrum of a continuous field function Φ can be found in Appendix B.

5. Numerical results

5.1. Code validation

Conceptually, all the examples considered in this section refer to 2D regions S like the ones displayed in figure 2 which are divided in two subregions S_1 and S_2. The various geometries of the regions that were analyzed are that of a circle, an ellipse and a square. Both homogeneous and non-homogeneous media are studied. For all these problems the domain of interest Ω is governed by the geometry of the region S and by a time interval $[0, T]$. This domain is partitioned using linear 3D cubic finite elements. Therefore a finite set of space-time points is

defined. A sinusoidal signal is applied at the center of the two dimensional partitioned region S with period 15 time units. The field evolution is solved via a finite difference scheme. The resulting field is sampled both in space and time at the space-time points defined by the apexes of the cubic domains and the samples are used as inputs to the model illustrated in the previous sections.
Lets consider a circular two dimensional region. A snapshot of a field generated by a central sinusoidal signal and calculated using a finite difference numerical scheme, is displayed in figure 8(a). By collecting all the sampled field values generated by this finite difference scheme in a vector $\{\Phi\}$ and solving directly equation 6 for $\{F\}$, the source producing the sampled field is reconstructed. A snapshot of this "revealed" source is displayed in figure. 8(b). Since the characteristics of this "revealed" source much with the characteristics of the initially imposed central sinusoidal source, a first indication of the validity of the algorithm is obtained. This source which produces the sampled field is called direct source.
The next step is to divide the domain Ω into two sub-domains. One that will be the support of the distributed source function (Ω_1) and another that will be the null set of the distributed source function (Ω_2) and in which the desired sampled field must be synthesized accurately. The values of the distributed constrained source function $\{F_{c1}\}$ are specified utilizing the aforementioned least squares optimization technique. This distributed constrained source synthesizes the sampled field with minimum error. A snapshot of this constrained source is displayed in figure 8(c). Finally, a snapshot of the field, generated by this constrained source is displayed in figure 8(d).

The main performance measures of this synthesis algorithm is the mean absolute error $\mu(|\epsilon|)$ between the initially sampled field and the generated by the constrained source field and its standard deviation $\sigma(|\epsilon|)$. These performance measures are evaluated for the whole domain Ω and for the sub-domains Ω_1 and Ω_2. The results are presented in the next tables, for various geometries, material properties and region dimensions.
In all the setups studied, cubic elements of side one unit in both space and time ($\Delta X = \Delta Y = \Delta T = 1$) were used.
Unless stated, the propagation velocity of the wave c_n inside each elemental domain $\Delta\Omega^{(n)}$ was chosen to be $c_n = \sqrt{\frac{k_n}{\rho_n}} = \sqrt{2}$. This was done by forcing $k_n = 2$ and $\rho_n = 1$. For simplicity and in order to study the effectiveness of the algorithm in media with different propagation velocities the material density was kept $\rho_n = 1$ while the modulus of elasticity k_n was varied. (For the coefficients k_n and ρ_n refer to equation (5)).

5.2. Problem-1: Circular region

A standard circular 2 dimensional region was studied first. A circular disk of radius 10 units containing an inner circular region of radius 4 units, was considered. Figure 9 displays this setup.

The base region for this problem consists of a total of 305 points of which 260 belong to region S_1 and 45 in S_2. Also it has 72 boundary points as figure 9 depicts. In order to build the space time domain we considered 16 frames (including the initial frame) resulting to 4880 total space-time points. These details are illustrated in table 5.2.
The synthesis algorithm was implemented using the wave field generated by a central sinusoidal signal of period 15 time units acting on a circular area of radius 2 space units for 16 time frames

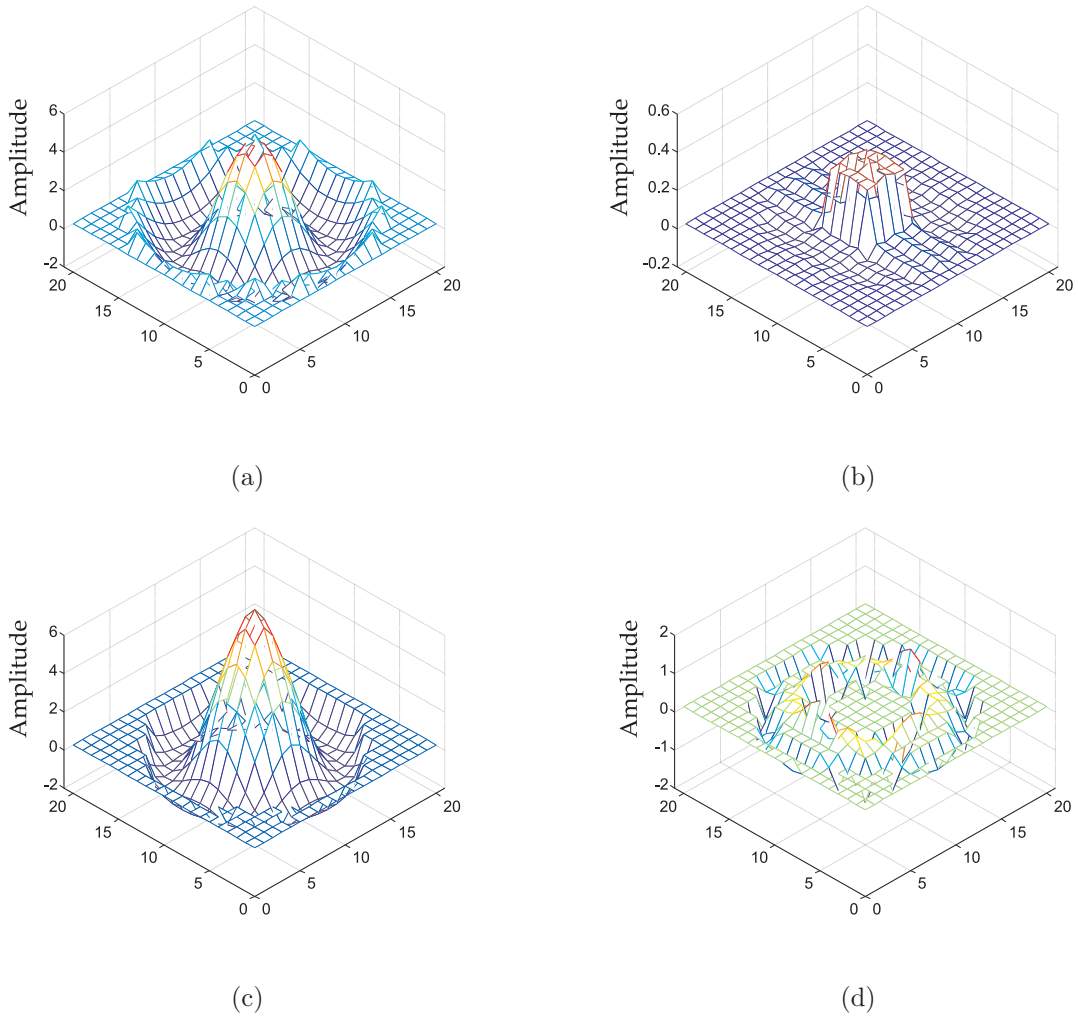

Figure 8. **Homogeneous circular region:** (a) Snapshot of the sampled wave field based on a finite difference scheme (b) Snapshot of the source distribution estimated from the algorithm (c) Snapshot of the reconstructed wave field by the constrained source (d) Snapshot of the constrained source

Region	Total Points	Inner Points	Boundary Points
Ω	4880	3262	1618
Ω_1	4160	2632	1528
Ω_2	720	630	90
S	305	233	72
S_1	260	188	72
S_2	45	45	0

Table I. **Circular region:** Partition details

(including the initial frame). A snapshot of the obtained error distribution across the circular region is displayed in figure 10.

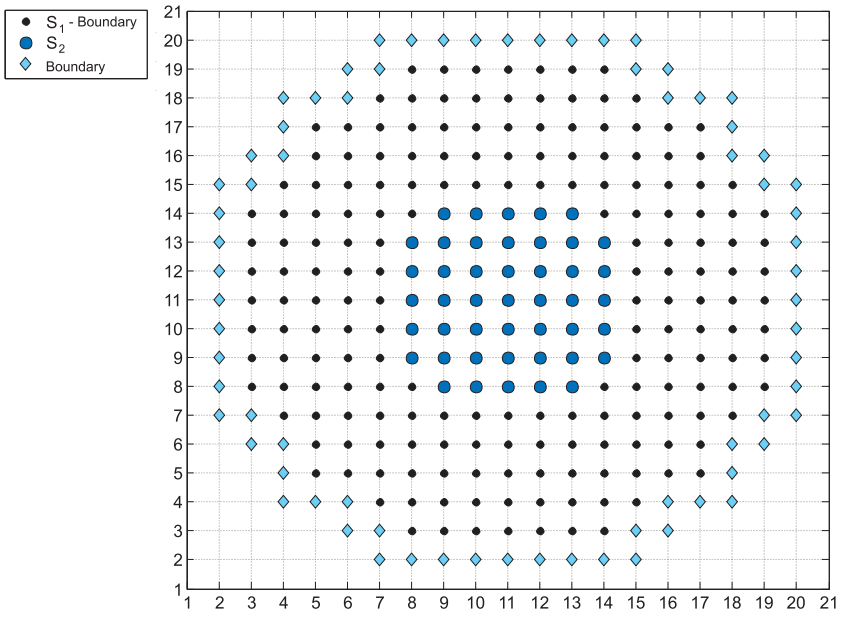

Figure 9. **Circular region:** Partition

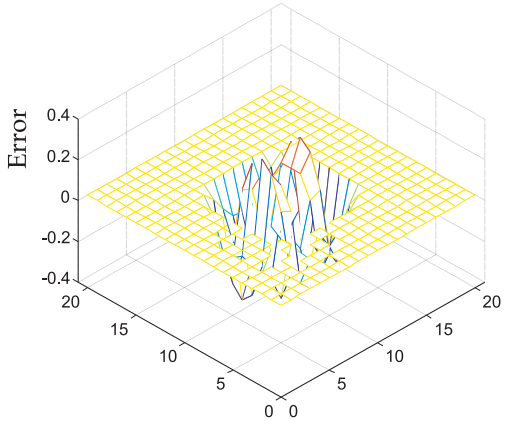

Figure 10. **Circular region:** Snapshot of the error distribution

5.3. Geometric effects: Different radii of the inner circular region

The synthesis algorithm was also implemented on the previous circular geometry using the wave field generated by the same central source signal for different radii of the inner circular region (S_2) ranging from 2 to 8 units. The radius of the outer region was kept constant at 10 space units. The observed maximum absolute value of the sampled field was $\max(|\Phi|) = 4.5796$. The results regarding the mean absolute error $\mu(|\epsilon|)$ and its standard deviation $\sigma(|\epsilon|)$ are summarized in table .

Radius of S_2	$\mu(\|\epsilon\|)$ in Ω	$\mu(\|\epsilon\|)$ in Ω_1	$\mu(\|\epsilon\|)$ in Ω_2	$\sigma(\|\epsilon\|)$ in Ω_1	$\sigma(\|\epsilon\|)$in Ω_2
8	0.6202	0.5705	0.6308	0.3197	0.5727
7	0.5153	0.2135	0.7005	0.2500	0.6260
6	0.4414	0.0864	0.8485	0.1446	0.6495
5	0.3826	0.0938	1.0731	0.2506	0.6780
4	0.3257	0.1289	1.1526	0.3845	0.6573
3	0.2074	0.1823	0.4177	0.3915	0.5708
2	0.0566	0.0402	0.4654	0.1828	0.3252

Table II. **Circular region:** Mean absolute error $\mu(|\epsilon|)$ and its standard deviation $\sigma(|\epsilon|)$ in Ω, Ω_1 and Ω_2, as a function of the radius of the inner circular region.

Based on the above table we see that both the mean errors in Ω and Ω_1 are reduced as the size of the inner region is reduced. This fact is expected. The constrained source is allowed to reside in more points as the inner region becomes smaller and therefore the synthesis results are better.

5.4. Variable weights

The synthesis algorithm was also applied minimizing a weighted total square error and using the wave field generated by the same central sinusoidal signal. Initially, a weight vector for error of the inner points of Ω_1 was formed $w_1 = \{w, ..., w\}$. Then, a weight vector for the error of the inner points of Ω_2 was calculated as $w_2 = \{s, ..., s\}$ with $s = \frac{|w_1|(1-w)+|w_2|}{|w_2|}$ according to 31, ($|x|$ refers to the number of elements of vector x). The parameter w was varied from 0.1 to 1. The obtained results are displayed in table III.

Based on table III we observe that as the weight of the inner points of the domain Ω_1 decreases, the mean absolute error in the domain Ω_2 decreases while the standard deviation remains approximately constant.

5.5. Problem-2: Elliptical region

The next examined geometry was an elliptical two dimensional region which is displayed in figure 11. Its characteristics are presented in table IV.
The synthesis algorithm was implemented, using the wave field generated by a sinusoidal central signal of period 15 time units, acting on an circular area of radius 1 space unit for 16 time frames (including the initial frame). Figure 12 shows a snapshot of the resulted error distribution.

Weight w of Ω_1	max($\|\Phi\|$)	$\mu(\|\epsilon\|)$ in Ω	$\mu(\|\epsilon\|)$ in Ω_1	$\mu(\|\epsilon\|)$ in Ω_2	$\sigma(\|\epsilon\|)$ in Ω_1	$\sigma(\|\epsilon\|)$ in Ω_2
0.1	4.5796	0.8516	0.8503	0.8570	2.4913	0.6737
0.2	4.5796	0.7377	0.7036	0.8803	2.1069	0.6506
0.3	4.5796	0.6029	0.5286	0.9131	1.6129	0.6293
0.4	4.5796	0.4946	0.3865	0.9459	1.1688	0.6204
0.5	4.5796	0.4127	0.2787	0.9730	0.8611	0.6210
0.6	4.5796	0.3621	0.2108	0.9942	0.6846	0.6238
0.7	4.5796	0.3397	0.1788	1.0120	0.5913	0.6251
0.8	4.5796	0.3325	0.1650	1.0325	0.5333	0.6229
0.9	4.5796	0.3320	0.1555	1.0692	0.4746	0.6203
1.0	4.5796	0.3271	0.1296	1.1526	0.3854	0.6573

Table III. **Circular region:**Mean absolute error $\mu(|\epsilon|)$ and its standard deviation $\sigma(|\epsilon|)$ in Ω, Ω_1 and Ω_2, as a function of the weight coefficient w.

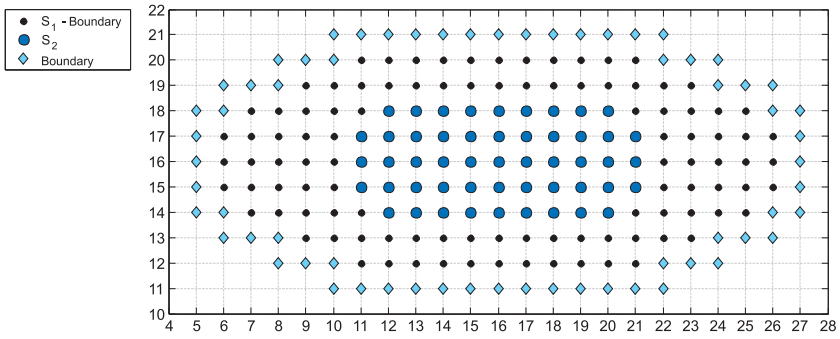

Figure 11. **Elliptical region:** Partition

Region	Total Points	Inner Points	Boundary Points
Ω	3472	2142	1330
Ω_1	2656	1428	1228
Ω_2	816	714	102
S	217	153	64
S_1	166	102	64
S_2	51	51	0

Table IV. **Elliptical region:** Partition details

5.5.1. Inhomogeneities In the previous elliptical domain, inhomogeneities were introduced by changing the propagation velocities at the points of the domain Ω_2 while keeping the velocities at the points in Ω_1 constant and vice versa. Table V shows how the maximum absolute value of the initial field, the maximum absolute value of the constrained source and the performance measure $\mu(|\epsilon|)$ change as we change the propagation velocity in one region while keeping it constant in the other region.

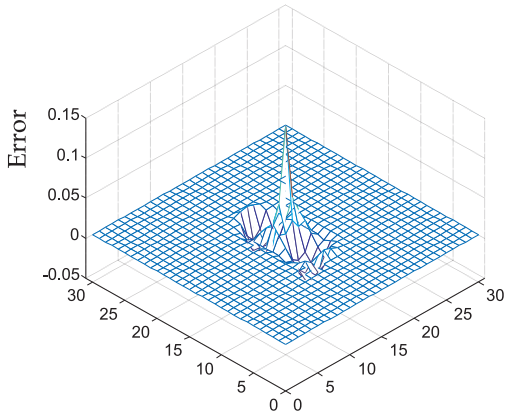

Figure 12. **Elliptical region:** Snapshot of the error distribution

c_2^2	max($\|\Phi\|$)	$\mu(\|\epsilon\|)$	max($\|F_1\|$)	c_1^2	max($\|\Phi\|$)	$\mu(\|\epsilon\|)$	max($\|F_1\|$)
0.50	0.4563	0.0252	0.3568	0.50	0.4563	0.0252	0.3568
0.45	0.4561	0.0248	0.3821	0.45	0.4829	0.0249	0.3675
0.40	0.4507	0.0239	0.4144	0.40	0.5072	0.0245	0.3685
0.35	0.4224	0.0224	0.5145	0.35	0.5033	0.0240	0.3578
0.30	0.4363	0.0222	0.5757	0.30	0.5441	0.0233	0.3550
0.25	0.4046	0.0246	0.7304	0.25	0.5431	0.0225	0.3744
0.20	0.3935	0.0226	0.7547	0.20	0.5794	0.0212	0.4923
0.15	0.6108	0.0264	1.0416	0.15	0.6423	0.0193	0.6660
0.10	0.4866	0.0403	3.3841	0.10	0.7626	0.0177	0.8195
0.05	0.8758	0.0685	5.6771	0.05	1.2808	0.0453	1.8382

Table V. **Elliptical region:** Maximum absolute value of the original field max($|\Phi|$), mean absolute error $\mu(|\epsilon|)$ in the whole domain Ω and maximum absolute value of the constrained source max($|F_1|$) in Ω_1, as a function of the propagation velocity in Ω_2 (assuming constant velocity in Ω_1 $c_1^2 = 0.5$) and vice versa.

5.5.2. Geometric effects: Scaling of inner elliptical region As we did in the circular geometry, the algorithm was implemented considering different dimensions of the inner elliptical region (S_2) and using the wave field generated by the same central sinusoidal signal (Radius: 1 space unit, Period: 15 time units) for 16 time frames (including the initial frame). The lengths of the minor and the major axis of the outer elliptical region were 6 and 12 space units respectively. The lengths of the axes of the inner elliptical region were varied keeping their ratio constant. The results are presented in table VI as a function of the minor and the major axis lengths of the inner elliptical region. The maximum absolute value of the sampled field was max($|\Phi|$) = 0.4563.

Minor/Major Axis	max($\|F_1\|$)	$\mu(\|\epsilon\|)$in Ω	$\mu(\|\epsilon\|)$in Ω_1	$\mu(\|\epsilon\|)$in Ω_2	$\sigma(\|\epsilon\|)$in Ω_1	$\sigma(\|\epsilon\|)$in Ω_2
1 / 2	0.4710	0.0030	0.0018	0.0612	0.0084	0.0788
2 / 4	0.4786	0.0042	0.0028	0.0346	0.0105	0.0568
3 / 6	0.4473	0.0144	0.0100	0.0333	0.0271	0.0387
4 / 8	0.4330	0.0165	0.0121	0.0284	0.0280	0.0348
5 / 10	0.3566	0.0300	0.0182	0.0411	0.0288	0.0372

Table VI. **Elliptical region:** Maximum value of the distributed source max($|F_1|$), mean absolute error $\mu(|\epsilon|)$ and its standard deviation $\sigma(|\epsilon|)$ in the domains Ω,Ω_1 and Ω_2 as a function of the lengths of the minor and the major axis of the inner elliptical region.

5.6. Problem-3: Square Region

The last considered geometry was a square two dimensional region displayed in figure 13 with characteristics summarized in table VII.

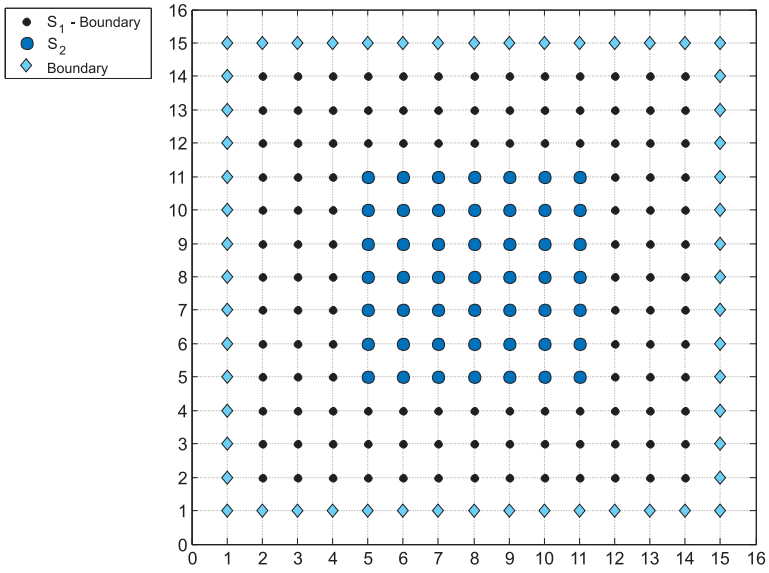

Figure 13. **Square region:** Partition

The synthesis algorithm was applied using the wave field generated by a central sinusoidal source acting on an circular area of radius 2 space units with period 15 time units for 16 time frames (including the initial frame). A snapshot of the obtained error distribution is displayed in figure 14.

5.6.1. Inhomogeneities Inhomogeneities were also considered in the square region. The synthesis algorithm was implemented using the wave field generated by the same central

Region	Total Points	Inner Points	Boundary Points
Ω	3600	2366	1234
Ω_1	2816	1680	1136
Ω_2	784	686	98
S	225	169	56
S_1	176	120	56
S_2	49	49	0

Table VII. **Square region:** Partition details

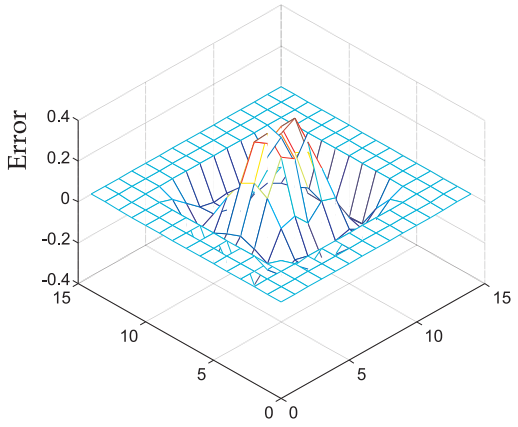

Figure 14. **Square region:** Snapshot of the error distribution

sinusoidal signal (Radius: 2 space units, Period: 15 time units) and changing the propagation velocities c_1 and c_2 of the two domains Ω_1 and Ω_2 respectively. The total considered time duration was again 16 time frames (including the initial frame). Table VIII displays the obtained results.

5.6.2. Geometric effects: Different sides of the inner square region The algorithm was also implemented for different side lengths of the inner square region (S_2) keeping the side length of the outer square region constant at 15 space units. The wave field generated by the same central sinusoidal signal (Radius: 2 space units, Period: 15 time units) for 16 time frames (including the initial frame) was used here again. The obtained results are summarized in table IX.

As we observed in the previous examples, in this case also the smaller the inner region is, the better the synthesis results are (smaller mean absolute error).

5.6.3. Variable attenuation coefficient Finally a change in the attenuation coefficient α was attempted. The coefficient was varied from 0 to 0.5 with step 0.05. The wave field used for the synthesis algorithm was the same field used in the previous considered cases of the square

c_2^2	max($\|\Phi\|$)	$\mu(\|\epsilon\|)$ in Ω	max($\|F_1\|$)	c_1^2	max($\|\Phi\|$)	$\mu(\|\epsilon\|)$ in Ω	max($\|F_1\|$)
0.50	2.2335	0.1940	1.6575	0.50	2.2335	0.1940	1.6575
0.45	2.1025	0.1831	1.6265	0.45	2.3585	0.1938	1.7016
0.40	2.0057	0.1688	1.5836	0.40	2.4898	0.1933	1.7075
0.35	1.9357	0.1520	1.8902	0.35	2.6210	0.1923	1.8598
0.30	1.9845	0.1357	2.6321	0.30	2.8039	0.1904	2.5016
0.25	2.1743	0.1220	3.9645	0.25	3.0475	0.1871	3.2449
0.20	2.7449	0.1210	7.1798	0.20	3.4500	0.1811	3.8363
0.15	2.3202	0.1916	13.2381	0.15	4.0989	0.1701	4.8138
0.10	1.3067	0.1075	11.4450	0.10	5.3899	0.1494	11.7534
0.05	3.3350	0.3391	57.7813	0.05	10.1976	0.1677	21.8417

Table VIII. **Square region:** Maximum absolute value of the original field max($|\Phi|$), mean absolute error $\mu(|\epsilon|)$ in the whole domain Ω and maximum value of the constrained source max($|F_1|$) in Ω_1, as a function of the propagation velocity in Ω_2 (assuming constant velocity in Ω_1 $c_1^2 = 0.5$) and vice versa.

Side	max($\|F_1\|$)	$\mu(\|\epsilon\|)$ in Ω	$\mu(\|\epsilon\|)$ in Ω_1	$\mu(\|\epsilon\|)$ in Ω_2	$\sigma(\|\epsilon\|)$ in Ω_1	$\sigma(\|\epsilon\|)$ in Ω_2
4	2.9199	0.0420	0.0331	0.2003	0.1182	0.2200
6	4.9576	0.1316	0.1181	0.2097	0.1833	0.2559
8	1.6575	0.1940	0.0766	0.4816	0.1796	0.2869
10	2.9633	0.2448	0.1751	0.3205	0.1435	0.2441
12	3.0932	0.2924	0.2253	0.3190	0.1789	0.2582

Table IX. **Square region:** Maximum absolute value of the distributed source max($|F_1|$), the mean absolute error $\mu(|\epsilon|)$ and its standard deviation $\sigma(|\epsilon|)$ in Ω, Ω_1 and Ω_2, as a function of the side length of the inner square region.

region. The results are presented in table X.

α	max($\|\Phi\|$)	$\mu(\|\epsilon\|)$ in Ω	$\mu(\|\epsilon\|)$ in Ω_1	$\mu(\|\epsilon\|)$ in Ω_2	$\sigma(\|\epsilon\|)$ in Ω_1	$\sigma(\|\epsilon\|)$ in Ω_2	max($\|F_1\|$)
0.00	2.2335	0.1940	0.0766	0.4816	0.1796	0.2869	1.6575
0.05	2.1695	0.1857	0.0725	0.4631	0.1679	0.2730	1.5546
0.10	2.1172	0.1787	0.0689	0.4476	0.1578	0.2621	1.4608
0.15	2.0717	0.1725	0.0657	0.4343	0.1487	0.2536	1.3747
0.20	2.0353	0.1669	0.0626	0.4223	0.1406	0.2472	1.2959
0.25	1.9983	0.1617	0.0596	0.4117	0.1333	0.2417	1.2242
0.30	1.9614	0.1568	0.0567	0.4018	0.1265	0.2374	1.1637
0.35	1.9250	0.1522	0.0540	0.3929	0.1201	0.2331	1.1086
0.40	1.8891	0.1477	0.0513	0.3840	0.1141	0.2299	1.0580
0.45	1.8539	0.1434	0.0487	0.3751	0.1085	0.2278	1.0578
0.50	1.8193	0.1390	0.0462	0.3663	0.1031	0.2261	1.0940

Table X. **Square region:** Maximum absolute value of the original field max($|\Phi|$) in Ω, mean absolute error $\mu(|\epsilon|)$ in Ω, Ω_1 and Ω_2 and maximum absolute value of the constrained source max($|F_1|$) as a function of different attenuation coefficients of the medium α.

6. Concluding Remarks

A formulation of distributed wave field synthesis with and without source constrains, in reference to a two dimensional medium has been developed. Material inhomogeneities and other non-linearities like dissipation are shown to be quite easy to handle in this formulation.

Also, a fully finite element scheme compared with a hybrid finite element in space and finite difference in time model, appears to be computationally easier when it is used to solve wave field synthesis problems. The main reason is that the knowledge of the field we want to synthesize before hand as vector $\{\Phi\}$ in space and time, constrains the required computations to be linear matrix calculations. Also, in such a scheme, the final solution is provided as a vector both in time and space.

Wave field synthesis has broad applications and involves extensive experimentation and cost. We presented a numerical approach based on inverse formulation with FEM [10],[11] to alleviate some of these concerns. The original signal corresponding to a given acoustic wave field distribution has been generated quite accurately with this scheme for both homogenous and non-homogeneous 2-D media. The method is straightforward to be extended to 3-D media with dissipation. The mesh size needed to capture the source distribution with a reasonable accuracy does indeed depend on the frequency and propagation velocity of the medium as one would expect. Finally, its essential to use various sparse algorithms [28] for the solution of the resultant linear system of equations as is done for this work here. The MATLAB code used to produce the results of the problems with the various geometries can be found at: http://cn.ece.cornell.edu/publications/papers/20060130/

7. Acknowledgements

The authors would like to express their sincere thanks to Prof. Subrata Mukherjee, Theoretical and Applied Mechanics Department, Cornell University for helpful discussions on the subject.

REFERENCES

1. A.J. Berkhout, D. de Vries P.Vogel "Acoustic Control By Wave field Synthesis" *Journal of Acoustic Society of America 93*, pp2764-2778 (1993).
2. M.M.Boon and E.N.G.Verheijen, "Multi-Channel Sound Reproduction Based on Wave Field Synthesis", 95^{th} *AES Convention 1993 October 7-10 New York.*
3. P.M.Morse, K.U.Ingard *Theoretical Acoustics*, McGraw-Hill, 1968.
4. L.E.Kinsler, A.R.Frey, A.B.Coppens and J.V.Sanders, *Fundamentals of Acoustics*, Wiley, 1999.
5. A.J. Berkhout, *Applied Seismic Wave Theory*, Elsevier, 1987.
6. A.F.Seybert, B.Soenarko, F.J.Rizzo, and D.J. Shippy, "An advanced computaional method for radiation and scattering of acoustic waves in three dimensions", *Journal of Acoustical Society of America*, 1985;77:362-68.
7. G.M.Hulbert, T.Hughes, "Space-time finite element methods for second-order hyperbolic equations",*Computer methods in Applied Mechanics and Engineering, no. 84, pp. 327-348, 1990.*
8. T.Hughes, G.M.Hulbert, "Space-time finite element methods for elastodynamics: formulations and error estimates",*Computer methods in Applied Mechanics and Engineering, no. 66, pp. 339-363, 1988.*
9. C. Johnson, "Discontinuous galerkin finite element methods for second order hyperbolic problems", *Computer methods in Applied Mechanics and Engineering, no. 107, pp. 117-129, 1993.*
10. O. Zienkievicz, *The Finite Element Method*, McGraw Hill.
11. T.Hughes, *The Finite Element Method, Linear Static and Dynamic Finite Element Analysis*, Dover Publications.

12. A.Rosen, M.A.Stuchly and A.V.Vorst, "Applications of RF/Microwaves in Medicine", *IEEE Transactions on Microwave Theory and Techniques*, vol. 50, Issue-3, 2002.
13. C.Lancaster, A.Toi, J.Trachtenberg, "Interstitial microwave thermoablation for localized prostate cancer", *Urology,* 1999;53: 828-831.
14. M.Sherar, J.Trachtenberg, M.Sean, R.Davidson, C.McCann, C.Yue, M.Haider, and M.Gertner, "Interstitial Microwave Thermal therapy for Prostate Cancer", *Journal of Endurology*, vol. 17, PP. 617-625, 2003.
15. T.Satoh,T.M.Seilhan, P.R.Stauffer, "Interstitial helical coil microwave antenna for experimental brain hyperthermia", *Neurosurgery*. 1988;23:564-569.
16. M.G.Skinner, M.N.Iizuka, M.C.Kolios, M.D.Sherar, "A theoretical comparison of energy sources-microwave, ultrasound and laser - for interstitial thermal therapy", *Phys Med Biol,* vol. 58, 1998;43:3535-3547.
17. J.Mendecki, E.Friedenthal, C.Botstein, "Microwave-induced hyperthermia in cancer treatment: Apparatus and preliminary results", *Int J Radiat Oncol Biol Phys,* 1978;4:1095-1103.
18. T.P. Ryan, "Comparison of six microwave antennas for hyperthermia treatment of cancer: SAR results for single antennas and arrays", *Int J Radiat Oncol Biol Phys,* 1991;21:403-413.
19. C.C.Vernon, J.W.Hand, S.B.Field, "Radiotherapy with or without hyperthermia in the treatment of superficial localized breast cancer: Results from five randomized controlled trials", *Int J Radiat Oncol Biol Phys*, 1996;35:731-744.
20. J.Van der Zee, G.D.Gonzalez, G.C. Van Rhoon, "Comparison of radiotherapy alone with radiotherapy plus hyperthermia in locally advanced pelvic tumours: A prospective, randomised, multicentre trial", *Lancet,* vol. 71, pp. 2000;355:1119-1125.
21. P.K.Sneed, P.R.Stauffer, M.W.McDermott, "Survival benefit of hyperthermia in a prospective randomized trial of brachytherapy boost 1/2 hyperthermia for glioblastoma multiforme", *Int J Radiat Oncol Biol Phys,* 1998;40:287-295.
22. Y.H.Pao and V.Varatharajulu, "Huygens' principle, Radiation Conditions and Integral Equations for the Scattering of Elastic waves", *Dept. of Theor. and Appl. MEch*, Cornell University, Ithaca, NY., USA, 1975.
23. V.D.Kupradze, "Potential Methods in the Theory of Elasticity", *Israel Programme for Scientific Translation*, Jerusulem, 1965.
24. S.Kobayashi, "Some applications of the boundary element method in elastodynamics", *BETECH 85*, Southampton, Computational Mechanics Publications, PP. 91-104, 1985.
25. K.F.Graff, *Wave motion in elastic solids* Ohio state university press, 1975
26. Y.Niwa, S.Kobayashi and T.Fukui, "Applications of the integral equation method to some geomechanical problems", *Numerical Methods in Geomechanics*, ASCE, PP. 120-131, 1976 (Vol 1).
27. I.Sanchez, J.R.Banga and A.A.Alonso, "Robust Identification and control of microwave heating processes", *7th International Conference on Microwave and HF Heating*,PP. 13-17, 1999.
28. T.F.Coleman and Y.Li, *Large-Scale Numerical Optimization*, Society for Industrial and Applied Mathematics, 1990.
29. G.N.Lilis, S.Telukunta, S.D.Servetto "Inverse Wave Field Synthesis" *17th International Symposium on Nonlinear Acoustics*, State College, PA, July 2005.
30. G.N.Lilis, S.D.Servetto "dWFS: Distributed Wave Field Synthesis" *IEEE International Conference on Acoustics, Speech, and Signal Processing (ICASSP)*, Toulouse, France, May 2006.

8. Appendix A

8.1. Derivation of the matrix form of the wave PDE

Given the definitions postulated in section 2, consider the Lagrange quantity L inside an arbitrary elemental domain $\Delta\Omega^{(n)}$ as a function of the field Φ and its partial derivatives in space and time as:

$$L(\Phi, \Phi_x, \Phi_y, \Phi_t) = \frac{1}{2}\rho_n \Phi_t^2 + a_n \Phi_t \Phi - \frac{1}{2}k_n[\Phi_x^2 + \Phi_y^2] + F\Phi \tag{33}$$

Consider the function $\Phi_c(x, y, t)$ satisfying (5) and an arbitrary function $\Phi(x, y, t)$, such that $(x, y, t) \in \Delta\Omega^{(n)}$. The deviation of $\Phi(x, y, t)$ from the function $\Phi_c(x, y, t)$, and its derivatives are given by:

$$\begin{aligned} \Delta\Phi(x,y,t) &= \Phi(x,y,t) - \Phi_c(x,y,t) & \Delta\Phi_t(x,y,t) &= \Phi_t(x,y,t) - \Phi_{ct}(x,y,t) \\ \Delta\Phi_x(x,y,t) &= \Phi_x(x,y,t) - \Phi_{cx}(x,y,t) & \Delta\Phi_y(x,y,t) &= \Phi_y(x,y,t) - \Phi_{cy}(x,y,t) \end{aligned} \tag{34}$$

Since L is a function of $\Phi, \Phi_x, \Phi_y, \Phi_t$ we can define the deviation of L as follows,

$$\Delta L = L(\Phi, \Phi_x, \Phi_y, \Phi_t) - L(\Phi_c, \Phi_{cx}, \Phi_{cy}, \Phi_{ct}) \tag{35}$$

From (33),(34) and (35) we can write compactly the deviation:

$$\begin{aligned} \Delta L &= \rho_n \Phi_{ct} \Delta\Phi_t + a_n \Phi_{ct} \Delta\Phi - k_n[\Phi_{cx}\Delta\Phi_x + \Phi_{cy}\Delta\Phi_y] + F\Delta\Phi + E \\ E &= \frac{\rho_n}{2}\Delta\Phi_t^2 + \alpha_n \Phi \Delta\Phi_t - \frac{k_n}{2}[\Delta\Phi_x^2 + \Delta\Phi_y^2] \end{aligned} \tag{36}$$

Integrating both sides of the previous equation within the elemental domain $\Delta\Omega^{(n)}$ we obtain:

$$\int_{\Delta\Omega^{(n)}} \Delta L d\omega = \int_{\Delta\Omega^{(n)}} \{\rho_n \Phi_{ct}\Delta\Phi_t + a_n \Phi_{ct}\Delta\Phi - k_n[\Phi_{cx}\Delta\Phi_x + \Phi_{cy}\Delta\Phi_y] + F\Delta\Phi\} d\omega + \int_{\Delta\Omega^{(n)}} E d\omega \tag{37}$$

Next we use integration by parts, and the fact that integrand functions are continuous and therefore the order of integration can be interchanged. Hence, by applying the integration by parts principle on the part that involves only partial derivatives of x we obtain:

$$\begin{aligned} &\int_{\Delta\Omega^{(n)}} \Delta\Phi_x \Phi_{cx} d\omega = \\ &\int_{t=t_n}^{t_n+\Delta T} \int_{y=y_n}^{y_n+\Delta Y} [\int_{x=x_n}^{x_n+\Delta X} \frac{\partial \Delta\Phi}{\partial x} \Phi_{cx} dx] dy dt = \\ &\int_{t=t_n}^{t_n+\Delta T} \int_{y=y_n}^{y_n+\Delta Y} [\Delta\Phi(\Phi_{cx})]\Big|_{x=x_n}^{x_n+\Delta X} dy dt - \int_{\Delta\Omega^{(n)}} \Delta\Phi \frac{\partial}{\partial x}[\Phi_{cx}] d\omega \end{aligned} \tag{38}$$

In more compact form and form definition 3 the previous equation can be written as:

$$\int_{\Delta\Omega^{(n)}} \Delta\Phi_x \Phi_{cx} d\omega = \int_{\Delta S^{(n)}_{+x}} [\Delta\Phi(\Phi_{cx})] dydt - \int_{\Delta S^{(n)}_{-x}} [\Delta\Phi(\Phi_{cx})] dydt - \int_{\Delta\Omega^{(n)}} \Delta\Phi \frac{\partial}{\partial x}[\Phi_{cx}] d\omega \tag{39}$$

Applying the previous property for the terms that include partial derivatives over y and t, collecting the resulting relations and combining them with (37) results to:

$$\begin{aligned}\int_{\Delta\Omega^{(n)}} \Delta L d\omega = \int_{\Delta\Omega^{(n)}} [\Delta\Phi(F + a_n\Phi_{ct} + k_n[\frac{\partial}{\partial x}(\Phi_{cx}) + \frac{\partial}{\partial y}(\Phi_{cy})] - \rho_n \frac{\partial}{\partial t}(\Phi_{ct}))] d\omega + \\ k_n[\int_{\Delta S^{(n)}_{+x}} [\Delta\Phi(\Phi_{cx})] dydt - \int_{\Delta S^{(n)}_{-x}} [\Delta\Phi(\Phi_{cx})] dydt + \\ \int_{\Delta S^{(n)}_{+y}} [\Delta\Phi(\Phi_{cy})] dxdt - \int_{\Delta S^{(n)}_{-y}} [\Delta\Phi(\Phi_{cy})] dxdt] + \\ \rho_n[\int_{\Delta S^{(n)}_{+t}} [\Delta\Phi(\Phi_{ct})] dxdy - \int_{\Delta S^{(n)}_{-t}} [\Delta\Phi(\Phi_{ct})] dxdy] + \int_{\Delta\Omega^{(n)}} E d\omega\end{aligned} \tag{40}$$

We know that for $\Phi = \Phi_c$ equation (5) is satisfied, therefore the volume integral in the second part of the last equation vanishes, leading to a simpler expression:

$$\begin{aligned}&\int_{\Delta\Omega^{(n)}} \Delta L d\omega = \\ &k_n[\int_{\Delta S^{(n)}_{+x}} [\Delta\Phi(\Phi_{cx})] dydt - \int_{\Delta S^{(n)}_{-x}} [\Delta\Phi(\Phi_{cx})] dydt + \int_{\Delta S^{(n)}_{+y}} [\Delta\Phi(\Phi_{cy})] dxdt - \int_{\Delta S^{(n)}_{-y}} [\Delta\Phi(\Phi_{cy})] dxdt] + \\ &\rho_n[\int_{\Delta S^{(n)}_{+t}} [\Delta\Phi(\Phi_{ct})] dxdy - \int_{\Delta S^{(n)}_{-t}} [\Delta\Phi(\Phi_{ct})] dxdy] + \int_{\Delta\Omega^{(n)}} E d\omega\end{aligned} \tag{41}$$

Finally utilizing (37)

$$\begin{aligned}&\int_{\Delta\Omega} \{\rho_n \Phi_{ct} \Delta\Phi_t + a_n \Phi_t \Delta\Phi - k_n[\Phi_{cx}\Delta\Phi_x + \Phi_{cy}\Delta\Phi_y] + F\Delta\Phi\} d\omega = \\ &k_n[\int_{\Delta S^{(n)}_{+x}} [\Delta\Phi(\Phi_{cx})] dydt - \int_{\Delta S^{(n)}_{-x}} [\Delta\Phi(\Phi_{cx})] dydt + \int_{\Delta S^{(n)}_{+y}} [\Delta\Phi(\Phi_{cy})] dxdt - \int_{\Delta S^{(n)}_{-y}} [\Delta\Phi(\Phi_{cy})] dxdt] + \\ &\rho_n[\int_{\Delta S^{(n)}_{+t}} [\Delta\Phi(\Phi_{ct})] dxdy - \int_{\Delta S^{(n)}_{-t}} [\Delta\Phi(\Phi_{ct})] dxdy]\end{aligned} \tag{42}$$

Equation (42) is the "weak" form of the 2 dimensional wave equation at the element level.

For example in the simple partition of the figure 15 we can write linear equations similar to (42) for each one of the elements $n = 1, 2, 3, 4$. If we sum the four equations for each element the intermediate surface integrals that appear in the second part will eliminate each other resulting to:

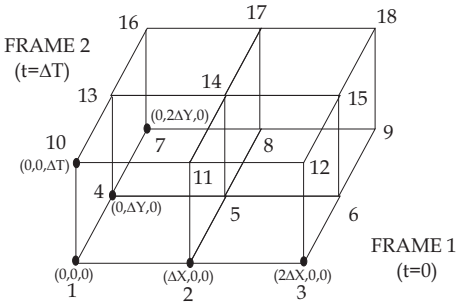

Figure 15. Partition into 4 elements

$$\sum_{n=1}^{4}\int_{\Delta\Omega^{(n)}}\{\rho_n\Phi_{ct}\Delta\Phi_t+a_n\Phi_{ct}\Delta\Phi-k_n[\Phi_{cx}\Delta\Phi_x+\Phi_{cy}\Delta\Phi_y]+F\Delta\Phi\}d\omega=$$
$$\int_{x=0}^{2\Delta X}\int_{y=0}^{2\Delta Y}\rho_n[\Delta\Phi[\Phi_{ct}]]\big|_{t=0}^{\Delta T}dydx-\int_{y=0}^{2\Delta Y}\int_{t=0}^{\Delta T}k_n[\Delta\Phi[\Phi_{cx}]]\big|_{x=0}^{2\Delta X}dtdy$$
$$-\int_{x=0}^{2\Delta X}\int_{t=0}^{\Delta T}k_n[\Delta\Phi[\Phi_{cy}]]\big|_{y=0}^{2\Delta y}dtdx \qquad (43)$$

We see that the second part of the previous equation contains surface integrals that refer to boundary surfaces of the partition and belong to only one element. Therefore to obtain a general expression for the partition $\bigcup_{n=1}^{4}\Delta\Omega^{(n)}$ we have to identify the subset of elements that have surfaces that do not belong to any other element in the partition. This kind of surfaces will contribute a surface integral after the assembly process in the second part of (43).

For each boundary element there is at least one boundary surface referring to it. Since we refer to 3 dimensions (two space and one time), we have 6 kinds of boundary surfaces (two per dimension). For example in x axis, there are boundary surfaces with their normal vector pointing out of the domain in either positive or negative direction.

From definition 6 the sets $N_{+x}, N_{-x}N_{+y}N_{-y}N_{+t}N_{-t}$ are the sets of elemental domains which contain boundary surfaces that belong to only on elemental domain which is a boundary elemental domain. In a general partition $\bigcup_{n=1}^{N}\Delta\Omega^{(n)}$ the surfaces that belong to these sets will contribute with one surface integral after the summation of all the equations like (42).

After summing equations like (42) written for every elemental domain one can conclude that:

$$\sum_{n=1}^{N}\int_{\Delta\Omega^{(n)}}\{\rho_n\Phi_{ct}\Delta\Phi_t+a_n\Phi_{ct}\Delta\Phi-k_n[\Phi_{cx}\Delta\Phi_x+\Phi_{cy}\Delta\Phi_y]+F\Delta\Phi\}d\omega=$$
$$\sum_{n\in N_{+t}}\int_{\Delta S^{(n)}_{+t}}\rho_n[\Delta\Phi[\Phi_{ct}]]dydx-\sum_{n\in N_{-t}}\int_{\Delta S^{(n)}_{-t}}\rho_n[\Delta\Phi[\Phi_{ct}]]dydx+$$
$$\sum_{n\in N_{+x}}\int_{\Delta S^{(n)}_{+x}}k_n[\Delta\Phi[\Phi_{cx}]]dtdy-\sum_{n\in N_{-x}}\int_{\Delta S^{(n)}_{-x}}k_n[\Delta\Phi[\Phi_{cx}]]dtdy+$$
$$\sum_{n\in N_{+y}}\int_{\Delta S^{(n)}_{+y}}k_n[\Delta\Phi[\Phi_{cy}]]dtdx-\sum_{n\in N_{-y}}\int_{\Delta S^{(n)}_{-y}}k_n[\Delta\Phi[\Phi_{cy}]]dtdx \tag{44}$$

8.2. Element Approximations

For the purpose of our investigation consider local coordinates (ξ,η,ζ) inside the elemental domain $\Delta\Omega^{(n)}$ satisfying $(\xi,\eta,\zeta)\in[-1,1]\times[-1,1]\times[-1,1]$ and

$$x(\xi)=x_n+\frac{\xi+1}{2}\Delta X\qquad y(\eta)=y_n+\frac{\eta+1}{2}\Delta Y\qquad t(\zeta)=t_n+\frac{\zeta+1}{2}\Delta T \tag{45}$$

Therefore linear approximations of $\Phi(x,y,t)$,$\Phi_c(x,y,t)$ and $\Delta\Phi(x,y,t)$ both in space and time can be defined by:

$$\Phi(\xi,\eta,\zeta)=\sum_{k=1}^{8}\phi_k^{(n)}N_k^{(n)}(\xi,\eta,\zeta)\qquad\qquad \Phi_c(\xi,\eta,\zeta)=\sum_{k=1}^{8}\phi_{ck}^{(n)}N_k^{(n)}(\xi,\eta,\zeta)$$
$$\Delta\Phi(\xi,\eta,\zeta)=\sum_{k=1}^{8}\Delta\phi_k^{(n)}N_k^{(n)}(\xi,\eta,\zeta)\qquad\qquad \Delta\phi_k^{(n)}=\phi_k^{(n)}-\phi_{ck}^{(n)} \tag{46}$$

with $\phi_k^{(n)}$ being the values of the field Φ at the apexes of the domain $\Delta\Omega^{(n)}$ as figure 16 displays. The notation $N_k^{(n)}(\xi,\eta,\zeta)$ is used for the standard hexahedral interpolation functions [11]. Assuming k_i to be the i^{th} digit of the dyadic expansion of the integer number $k-1$ the values $\phi_k^{(n)}$ and the functions $N_k^{(n)}(\xi,\eta,\zeta)$ can be written as:

$$\phi_k^{(n)}=\Phi(x_n+k_1\Delta X,y_n+k_2\Delta Y,t_n+k_3\Delta T)\qquad k\in\{1,...,8\}$$
$$N_k^{(n)}(\xi,\eta,\zeta)=\frac{1}{8}[1+(-1)^{k_1+1}\xi][1+(-1)^{k_2+1}\eta][1+(-1)^{k_3+1}\zeta] \tag{47}$$

Based on the previous approximations we can write the partial derivatives of the field Φ and the partial derivatives of the difference $\Delta\Phi$ as:

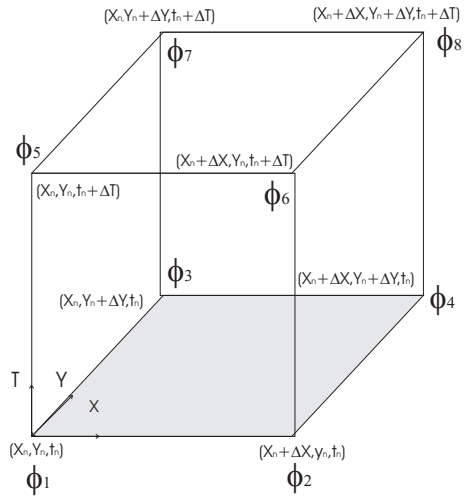

Figure 16. Cubic elemental domain

$$\Phi_x = \sum_{k=1}^{8} \phi_k^{(n)} \frac{\partial N_k^{(n)}}{\partial x} \qquad \Delta\Phi_x = \sum_{k=1}^{8} \Delta\phi_k^{(n)} \frac{\partial N_k^{(n)}}{\partial x}$$
$$\Phi_y = \sum_{k=1}^{8} \phi_k^{(n)} \frac{\partial N_k^{(n)}}{\partial y} \qquad \Delta\Phi_y = \sum_{k=1}^{8} \Delta\phi_k^{(n)} \frac{\partial N_k^{(n)}}{\partial y}$$
$$\Phi_t = \sum_{k=1}^{8} \phi_k^{(n)} \frac{\partial N_k^{(n)}}{\partial t} \qquad \Delta\Phi_t = \sum_{k=1}^{8} \Delta\phi_k^{(n)} \frac{\partial N_k^{(n)}}{\partial t} \tag{48}$$

Additionally we approximate the source function $F(\xi, \eta, \zeta)$ by a constant inside the elemental domain $\Delta\Omega^{(n)}$:

$$F(\xi, \eta, \zeta) = f^{(n)} \qquad \forall (\xi, \eta, \zeta) \in \Delta\Omega^{(n)} \tag{49}$$

The next goal is to evaluate the integrals of the interpolation functions and their derivatives in order to write (44) in a matrix form, given the approximations of (46),(48) and (49).
In order to do that, the following notation is introduced.
Given a positive integer number k we denote:
With $d_i(k)$ the i-th digit of the dyadic expansion of the integer k-1.
With $D_i(k)$ the dyadic expansion of the integer k-1 without the i-th digit.
With the symbol " $\oplus$ " the bitwise XOR operation between dyadic expansions.
For example: $110 \oplus 001 = 3$.

Utilizing (47) and the transformations of (45) the integrals of the interpolation functions and their derivatives can be written as:

$$\int_{\Delta\Omega^{(n)}} N_m^{(n)} d\omega = \frac{1}{8}\Delta\Omega$$
$$\int_{\Delta\Omega^{(n)}} \frac{\partial N_m^{(n)}}{\partial x}\frac{\partial N_k^{(n)}}{\partial x} d\omega = \frac{(-1)^{d_1(m)+d_1(k)}}{3^2 2^{D_1(m)\oplus D_1(k)}}\frac{\Delta\Omega}{\Delta X^2}$$
$$\int_{\Delta\Omega^{(n)}} \frac{\partial N_m^{(n)}}{\partial y}\frac{\partial N_k^{(n)}}{\partial y} d\omega = \frac{(-1)^{d_2(m)+d_2(k)}}{3^2 2^{D_2(m)\oplus D_2(k)}}\frac{\Delta\Omega}{\Delta Y^2}$$
$$\int_{\Delta\Omega^{(n)}} \frac{\partial N_m^{(n)}}{\partial t}\frac{\partial N_k^{(n)}}{\partial t} d\omega = \frac{(-1)^{d_3(m)+d_3(k)}}{3^2 2^{D_3(m)\oplus D_3(k)}}\frac{\Delta\Omega}{\Delta T^2}$$
$$\int_{\Delta\Omega^{(n)}} N_m^{(n)}\frac{\partial N_k^{(n)}}{\partial t} d\omega = \frac{(-1)^{d_3(k)+1}}{3^2 2^{D_3(m)\oplus D_3(k)+1}}\Delta X\Delta Y$$
$$\int_{\Delta S_{+x}^{(n)}} [N_m^{(n)}\frac{\partial N_k^{(n)}}{\partial x}] dydt - \int_{\Delta S_{-x}^{(n)}} [N_m^{(n)}\frac{\partial N_k^{(n)}}{\partial x}] dydt = \frac{(-1)^{d_1(m)+d_1(k)}}{3^2 2^{D_1(m)\oplus D_1(k)}}\frac{\Delta Y\Delta T}{\Delta X}$$
$$\int_{\Delta S_{+y}^{(n)}} [N_m^{(n)}\frac{\partial N_k^{(n)}}{\partial y}] dxdt - \int_{\Delta S_{-y}^{(n)}} [N_m^{(n)}\frac{\partial N_k^{(n)}}{\partial y}] dxdt = \frac{(-1)^{d_2(m)+d_2(k)}}{3^2 2^{D_2(m)\oplus D_2(k)}}\frac{\Delta X\Delta T}{\Delta Y}$$
$$\int_{\Delta S_{+t}^{(n)}} [N_m^{(n)}\frac{\partial N_k^{(n)}}{\partial t}] dxdy - \int_{\Delta S_{-t}^{(n)}} [N_m^{(n)}\frac{\partial N_k^{(n)}}{\partial t}] dxdy = \frac{(-1)^{d_3(m)+d_3(k)}}{3^2 2^{D_3(m)\oplus D_3(k)}}\frac{\Delta X\Delta Y}{\Delta T} \quad (50)$$

In the approximations of (46),(48) and (49), the notation $\phi_k^{(n)}$ is used for the field values and the notation $\Delta\phi_m^{(n)}$ for the variations of these values. The superscript (n) refer to the index of the element and the subscript m or k to the local (in the element) index of the specific point. Since different indices in (44) sometimes refer to the same space-time point it is useful to define a mapping function between the local indices of the points in the elements and the global indices of these points in the whole domain.
Let us consider a generic domain of a total of G global space-time points. Assume also in this domain, that there are N total elements. Then a mapping function can be defined as:

$$T : \{1, ..., 8\} \times \{1, .., N\} \rightarrow \{1, ..., G\} \quad (51)$$

Under the above mapping and based on the "volume" integrals that appear in (44) and the integrals of (50), a global matrix $[A^{(G)}]$ can be constructed as:

$$[A_{ij}^{(G)}] = \sum_{n=1}^{N}\sum_{m=1}^{8}\sum_{k=1}^{8} \mathbf{I}(T(m,n)=i)\mathbf{I}(T(k,n)=j)[A_{mk}^{(n)}]$$
$$[A_{mk}^{(n)}] = \rho_n \frac{(-1)^{d_3(m)+d_3(k)}}{3^2 2^{D_3(m)\oplus D_3(k)}}\frac{\Delta\Omega}{\Delta T^2} + a_n \frac{(-1)^{d_3(k)+1}}{3^2 2^{D_3(m)\oplus D_3(k)+1}}\Delta X\Delta Y -$$
$$k_n[\frac{(-1)^{d_1(m)+d_1(k)}}{3^2 2^{D_1(m)\oplus D_1(k)}}\frac{\Delta\Omega}{\Delta X^2} + \frac{(-1)^{d_2(m)+d_2(k)}}{3^2 2^{D_2(m)\oplus D_2(k)}}\frac{\Delta\Omega}{\Delta Y^2}]$$

where $\mathbf{I}$ is the identity function.

Based on the "surface" integrals that appear in (44) and the integrals of (50), a global matrix $[B^{(G)}]$ can be also constructed.

$$[B_{ij}^{(G)}] = \sum_{n=1}^{N}\sum_{m=1}^{8}\sum_{k=1}^{8}\mathbf{I}(T(m,n)=i)\mathbf{I}(T(k,n)=j)B_{mk}^{(n)}$$

$$\begin{aligned} B_{mk}^{(n)} = \quad & \mathbf{I}(n\in N_{+x})[B_{(+x)mk}^{(n)}] - \mathbf{I}(n\in N_{-x})[B_{(-x)mk}^{(n)}] + \\ & \mathbf{I}(n\in N_{+y})[B_{(+y)mk}^{(n)}] - \mathbf{I}(n\in N_{-y})[B_{(-y)mk}^{(n)}] + \\ & \mathbf{I}(n\in N_{+t})[B_{(+t)mk}^{(n)}] - \mathbf{I}(n\in N_{-t})[B_{(-t)mk}^{(n)}] \end{aligned}$$

$$[B_{(+x)mk}^{(n)}] = \mathbf{I}(d_1(m)=1)k_n\frac{(-1)^{d_1(k)+1}}{3^2 2^{D_1(m)\oplus D_1(k)}}\frac{\Delta Y\Delta T}{\Delta X}$$

$$[B_{(-x)mk}^{(n)}] = \mathbf{I}(d_1(m)=0)k_n\frac{(-1)^{d_1(k)+1}}{3^2 2^{D_1(m)\oplus D_1(k)}}\frac{\Delta Y\Delta T}{\Delta X}$$

$$[B_{(+y)mk}^{(n)}] = \mathbf{I}(d_2(m)=1)k_n\frac{(-1)^{d_2(k)+1}}{3^2 2^{D_2(m)\oplus D_2(k)}}\frac{\Delta X\Delta T}{\Delta Y}$$

$$[B_{(-y)mk}^{(n)}] = \mathbf{I}(d_2(m)=0)k_n\frac{(-1)^{d_2(k)+1}}{3^2 2^{D_2(m)\oplus D_2(k)}}\frac{\Delta X\Delta T}{\Delta Y}$$

$$[B_{(+t)mk}^{(n)}] = \mathbf{I}(d_3(m)=1)\rho_n\frac{(-1)^{d_3(k)+1}}{3^2 2^{D_3(m)\oplus D_3(k)}}\frac{\Delta X\Delta Y}{\Delta T}$$

$$[B_{(-t)mk}^{(n)}] = \mathbf{I}(d_3(m)=0)\rho_n\frac{(-1)^{d_3(k)+1}}{3^2 2^{D_3(m)\oplus D_3(k)}}\frac{\Delta X\Delta Y}{\Delta T}$$

Under the same principles the global source vector $\{F_i^{(G)}\}$ can be constructed as:

$$\{F_i^{(G)}\} = \sum_{n=1}^{N}\sum_{m=1}^{8}\mathbf{I}[T(m,n)=i]\{F_m^{(n)}\} \qquad \{F_m^{(n)}\} = f^{(n)}\int_{\Delta\Omega^{(n)}} N_m^{(n)}d\omega = \frac{f^{(n)}\Delta\Omega}{8}$$

Finally the field vector and its variance will take the form of:

$$\{\Phi^{(G)}\} = [\phi_1,...,\phi_G]^T \qquad \{\Delta\Phi^{(G)}\} = [\Delta\phi_1,...,\Delta\phi_G]^T$$

Our next step is to sabstitute (48),(49),(46) in (44) and interchange the summations of equations (48),(49),(46) with the integrations of (44). Then, using the calculated integrals of (50), equation (44) can be written in a more compact form as:

$$\{\Delta\Phi^{(G)}\}^T\{[K^{(G)}]\{\Phi^{(G)}\} + \{F^{(G)}\}\} = \{0\} \qquad [K^{(G)}] = [A^{(G)}] - [B^{(G)}]$$

Note that the differences $\Delta\phi_g$ $(g = 1,...,G)$ "extracted" in $\{\Delta\Phi^{(G)}\}$ come from either the term $\Delta\Phi$ or the terms $\Delta\Phi_x$, $\Delta\Phi_y$, $\Delta\Phi_t$, appearing in (44).
The last equation must hold for every small variations of $\Delta\phi_g$, therefore the final matrix form can be obtained as:

$$[K^{(G)}]\{\Phi^{(G)}\} + \{F^{(G)}\} = \{0\} \tag{52}$$

9. Appendix B

9.1. Linear interpolation error

Consider a continuous square integrable function $F : S \times [0,T] \rightarrow \mathbf{R}$, where S is a two dimensional region and $[0,T]$ is a predefined time interval, like the one in figure 2. Given the region S there is always a rectangular cover of dimensions L_x, L_y encompassing the region S. Similarly we can define a cover Ω_E for the domain Ω. Both covers are displayed in figure 17 and their dimensions are chosen to be multiples of the dimensions ΔX,ΔX and ΔY of the elemental domains $\Delta\Omega^{(n)}$. In this way the cover Ω_E can be partitioned into a finite number of elemental domains $\Delta\Omega^{(n)}$ displayed also in figure 17.

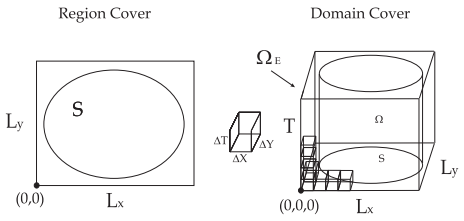

Figure 17. Region and domain cover

Based on the domain cover we can define a family of basis functions $N(x,y,t)$ as follows:

$$N_k^{(nmp)} = [k_1 \cos(\frac{n\pi x}{L_x}) + \bar{k_1} \sin(\frac{n\pi x}{L_x})][k_2 \cos(\frac{m\pi y}{L_y}) + \bar{k_2} \sin(\frac{m\pi y}{L_y})][k_3 \cos(\frac{p\pi t}{T}) + \bar{k_3} \sin(\frac{p\pi t}{T})] \tag{53}$$

where again $k \in \{1,2,...,8\}$ and $k_i, i = 1,2,3$ is the i^{th} digit of the dyadic expansion of the integer $k-1$ and $\bar{k_i}$ its complement. Additionally $n,m,p \in \{1,2,3,4,...\}$.

Since the initial function $F(x,y,t)$ is square integrable, it can be expanded as an infinite linear combination of the above basis functions. Furthermore since $\Omega \subset \Omega_E$ we force $F(x,y,t) = 0, \forall (x,y,t) \in \Omega_E - \Omega$.

If we consider a subset of the initial functions F such that the contribution of the higher order basis functions $(n > N, m > M, p > P)$ in this linear combination is negligible then:

$$\begin{aligned} F(x,y,t) &\approx \sum_{k=1}^{8} \sum_{n,m,p=0}^{N,M,P} c_k^{(nmp)} N_k^{(nmp)}(x,y,t) \\ c_k^{(nmp)} &= \frac{8}{L_x L_y T} \int_{\Omega_E} F(x,y,t) N_k^{(nmp)}(x,y,t) d\omega \end{aligned} \tag{54}$$

Lets define the operator $\mathbb{L}$ which acts on the function $F(x,y,t)$ and gives a linear interpolated version of this function based in its values at the grid points defined in definition 5. Assume also for simplicity that the elemental domains have side $(\Delta X = \Delta Y = \Delta T = a)$. Since the operator

is linear and acts on a function $F(x,y,t)$ that can be represented as a linear combination (54) then clearly:

$$\mathbb{L}[F(x,y,t)] \approx \sum_{k=1}^{8} \sum_{n,m,p=0}^{N,M,P} c_k^{(nmp)} \mathbb{L}[N_k^{(nmp)}(x,y,t)] \tag{55}$$

Now if we choose the side of the elemental domains a, in a way that the sides of the cover Ω_E are multiples of a then we can write that $L_x = a(Q+1)$,$L_y = a(R+1)$ and $T = a(S+1)$. In this way the whole cover is partitioned resulting to a total number of $A_{tot} = QRS$ elemental domains defined by the sets:

$$\Delta\Omega_{lqr} = [qa,(q+1)a] \times [ra,(r+1)a] \times [sa,(s+1)a]$$

with $q \in \{0,...,Q\}$ $\quad r \in \{0,...,R\}$ $\quad s \in \{0,...,S\}$.

According to equation (47), interpolation functions $G_{l(qrs)}(x,y,t)$ using global coordinates for every elemental domain $\Delta\Omega_{qrs}$ can be developed. Therefore the "action" of the operator $\mathbb{L}$ on the function $N_k^{(nmp)}(x,y,t)$ can be described by:

$$\begin{aligned}
&\mathbb{L}[N_k^{(nmp)}(x,y,t)] = \sum_{l=1}^{8} g_{l(qrs)}^{(nmp)} G_{l(qrs)}(x,y,t) \qquad \forall (x,y,t) \in \Delta\Omega_{qrs} \\
&g_{l(qrs)}^{(nmp)} = N_k^{(nmp)}(qa + l_1 a, ra + l_2 a, sa + l_3 a) \qquad l \in \{0,...,7\} \\
&G_{l(qrs)}(x,y,t) = [\bar{l_1} + (-1)^{l_1+1}(\frac{x}{a} - q)][\bar{l_2} + (-1)^{l_2+1}(\frac{y}{a} - r)][\bar{l_3} + (-1)^{l_3+1}(\frac{t}{a} - s)]
\end{aligned} \tag{56}$$

where l_1, l_2, l_3 are the digits of the dyadic expansion of the integer number $l-1, l \in \{1,...,8\}$.

Denoting $\Omega_E = [0,L_x] \times [0,L_y] \times [0,T]$ as the cover of the domain Ω and assuming that L_x, L_y, T are all multiples of the side a, a good measure for the error the interpolation induces, is given by the integral of the square of the difference between each basis function $N_k^{(nmp)}(x,y,t)$ and its interpolated version in Ω_E.

$$E = \sum_{k=0}^{7} \sum_{n,m,p=0}^{N,M,P} [c_k^{(nmp)}]^2 E_k^{(nmp)} \qquad E_k^{(nmp)} = \int_{\Omega_E} \{N_k^{(nmp)} - \mathbb{L}[N_k^{(nmp)}]\}^2 d\omega \tag{57}$$

Each of the $E_k^{(nmp)}$ is a component of the total square error. We can divide the integral of the component of the square error $E_k^{(nmp)}$ in (57) into sums of integrals in the elemental domains as:

$$E_k^{(nmp)} = \sum_{q,r,s=0}^{QRS} \int_{\Delta\Omega_{qrs}} \{N_k^{(nmp)} - \mathbb{L}[N_k^{(nmp)}]\}^2 d\omega \tag{58}$$

Lets concentrate on the integral inside the domain $\Delta\Omega_{qrs}$.

The square difference $\{N_k^{(nmp)} - \mathbb{L}[N_k^{(nmp)}]\}^2$ in the domain $\Delta\Omega_{qrs}$ can be written as:

$$\begin{aligned}
&\{N_k^{(nmp)} - \mathbf{L}[N_k^{(nmp)}]\}^2 = \\
&= \{N_k^{(nmp)} - \sum_{l=1}^{8} g_{l(qrs)}^{(nmp)} G_{l(qrs)}\}^2 \\
&= [N_k^{(nmp)}]^2 - 2N_k^{(nmp)} \sum_{l=1}^{8} g_{l(qrs)}^{(nmp)} G_{l(qrs)} + \sum_{l=1}^{8}\sum_{l'=1}^{8} g_{l(qrs)}^{(nmp)} g_{l'(qrs)}^{(nmp)} G_{l(qrs)} G_{l'(qrs)}
\end{aligned} \tag{59}$$

Therefore in order to evaluate the integral of the square of the difference in the domain $\Delta\Omega_{qrs}$ we have to evaluate the three following integrals:

$$\begin{aligned}
A_{k(qrs)}^{(nmp)}(a) &= \int_{\Delta\Omega_{qrs}} [N_k^{(nmp)}]^2 d\omega \\
B_{kl(qrs)}^{(nmp)}(a) &= \int_{\Delta\Omega_{qrs}} [N_k^{(nmp)} G_{l(qrs)}] d\omega \\
C_{ll'(qrs)}(a) &= \int_{\Delta\Omega_{qrs}} [G_{l(qrs)} G_{l'(qrs)}] d\omega
\end{aligned} \tag{60}$$

In these integrals the integration can be applied separately along the x, y, t axis because the integrands are functions that can be written as products of functions of x with functions of y and with functions of t.

Therefore we can write:

$$
\begin{aligned}
&A^{(nmp)}_{k(qrs)}(a) = XA^{(n)}_{k(q)} YA^{(m)}_{k(r)} TA^{(p)}_{k(s)} \\
&XA^{(n)}_{k(q)} = \frac{a}{2} + \frac{L_x}{4n\pi}[(k_1 - \bar{k_1})\sin(\frac{2n\pi}{L_x}x)]^{(q+1)a}_{qa} \\
&YA^{(m)}_{k(r)} = \frac{a}{2} + \frac{L_y}{4m\pi}[(k_2 - \bar{k_2})\sin(\frac{2m\pi}{L_y}y)]^{(r+1)a}_{ra} \\
&TA^{(p)}_{k(s)} = \frac{a}{2} + \frac{T}{4p\pi}[(k_3 - \bar{k_3})\sin(\frac{2p\pi}{T}t)]^{(s+1)a}_{sa} \\
&B^{(nmp)}_{kl(qrs)}(a) = XB^{(n)}_{kl(q)} YB^{(m)}_{kl(r)} TB^{(p)}_{kl(s)} \\
&XB^{(n)}_{kl(q)} = \frac{L_x}{n\pi}[\sin(\frac{n\pi}{L_x}x)(k_1(\bar{l_1} + (-1)^{l_1}q - x\frac{(-1)^{l_1}}{a}) - \bar{k_1}\frac{L_x}{n\pi}\frac{(-1)^{l_1}}{a}) + \\
&\qquad \cos(\frac{n\pi}{L_x}x)(k_1\frac{L_x}{n\pi}\frac{(-1)^{l_1+1}}{a} - \bar{k_1}(\bar{l_1} + (-1)^{l_1}q - x\frac{(-1)^{l_1}}{a}))]^{(q+1)a}_{qa} \\
&YB^{(m)}_{kl(r)} = \frac{L_y}{m\pi}[\sin(\frac{m\pi}{L_y}y)(k_2(\bar{l_2} + (-1)^{l_2}r - y\frac{(-1)^{l_2}}{a}) - \bar{k_2}\frac{L_y}{m\pi}\frac{(-1)^{l_2}}{a}) + \\
&\qquad \cos(\frac{m\pi}{L_y}y)(k_2\frac{L_y}{m\pi}\frac{(-1)^{l_2+1}}{a} - \bar{k_2}(\bar{l_2} + (-1)^{l_2}r - y\frac{(-1)^{l_2}}{a}))]^{(r+1)a}_{ra} \\
&TB^{(p)}_{kl(s)} = \frac{T}{p\pi}[\sin(\frac{p\pi}{T}t)(k_3(\bar{l_3} + (-1)^{l_3}s - t\frac{(-1)^{l_3}}{a}) - \bar{k_3}\frac{T}{p\pi}\frac{(-1)^{l_3}}{a}) + \\
&\qquad \cos(\frac{p\pi}{T}t)(k_3\frac{T}{p\pi}\frac{(-1)^{l_3+1}}{a} - \bar{k_3}(\bar{l_3} + (-1)^{l_3}s - t\frac{(-1)^{l_3}}{a}))]^{(s+1)a}_{sa} \\
&C_{ll'(qrs)}(a) = \prod_{i=1}^{3}\{A_{l_i l'_i x_i}(a) + B_{l_i l'_i x_i}(a) + C_{l_i l'_i x_i}(a)\} \\
&A_{l_i l'_i x_i}(a) = (\bar{l_i} + (-1)^{l_i}x_i)(\bar{l'_i} + (-1)^{l'_i}x_i)a \\
&B_{l_i l'_i x_i}(a) = [(\bar{l_i} + (-1)^{l_i}x_i)(-1)^{l'_i+1} + (\bar{l'_i} + (-1)^{l'_i}x_i)(-1)^{l_i+1}]\frac{2x_i+1}{2}a \\
&C_{l_i l'_i x_i}(a) = (-1)^{l_i+l'_i}\frac{(x_i+1)^3 - x_i^3}{3}aC_{l_i l'_i x_i} \\
&x_1 = q \quad x_2 = r \quad x_3 = s
\end{aligned}
\tag{61}
$$

Finally combining equations (57), (58) ,(59) and (60) we conclude that:

$$
\begin{aligned}
&E = \sum_{m,n,p=0}^{N,M,P}\sum_{k=1}^{8}\{[c_k^{(nmp)}]^2\sum_{q,r,s=0}^{Q,R,S} ABC^{(nmp)}_{k(qrs)}\} \\
&ABC^{(nmp)}_{k(qrs)} = A^{(nmp)}_{k(qrs)}(a) - 2\sum_{l=1}^{8} g^{(nmp)}_{l(qrs)} B^{(nmp)}_{kl(qrs)}(a) + \sum_{l=1}^{8}\sum_{l'=1}^{8} g^{(nmp)}_{l(qrs)} g^{(nmp)}_{l'(qrs)} C_{ll'(qrs)}(a)
\end{aligned}
\tag{62}
$$

In order to see how the error components change as the sampling step a and the frequency (determined by the triplet (n, m, p)) change we consider the case where $k = 1$ $L_x = L_y = T =$

10.

Then we plot the coefficients E_{nmp} for $a = 1$ (1000 elements), $a = 0.5$ (8000 elements) and 0.25 (64000 elements).
Since $N_k^{(nmp)}(x, y, t) = \cos(\frac{n\pi x}{L_x}) \cos(\frac{m\pi y}{L_y}) \cos(\frac{p\pi t}{T})$ and due to symmetry:

$E_{iij} = E_{iji} = E_{jii}$ therefore for $n, m, p \in \{1, 2, ..., 5\}$ we have to calculate only the components that appear in table 9.1.

E_{nmp}	$a = 1$	$a = 0.5$	$a = 0.25$
E_{111}	0.079300	0.005000	0.000316
E_{112}	0.321200	0.020700	0.001300
E_{122}	0.692700	0.045500	0.002900
E_{222}	1.184100	0.079300	0.005000
E_{223}	2.325000	0.162100	0.010200
E_{233}	3.731500	0.272300	0.017000
E_{333}	5.363700	0.404900	0.025400
E_{334}	8.117200	0.614200	0.040300
E_{344}	11.206800	0.914700	0.058300
E_{444}	14.490400	1.235100	0.079300
E_{445}	19.246600	1.648100	0.111700
E_{455}	24.122600	2.267500	0.149000
E_{555}	29.042400	2.875900	0.191100

Table XI. Error components E_{nmp} as a function of the sampling step a.

By looking in table 9.1 it is clear that as the sampling step reduces to half the component of the square error is multiplied by $\frac{1}{16}$. Therefore the total error is reduced by $\frac{1}{4}$.